Article

Erythroid SLC7A5/SLC3A2 amino acid carrier controls red blood cell size and maturation

Control mice

Aas

SLC3A2

SLC7A5

CD71

Aas

Ter119

mTORC1

Mitochondrial activity

Hemoglobin content

Erythroid precursor

Ter119

Hemoglobin content

Mature red blood cell

Erythroid Slc7a5-deficient mice

CD71

Ter119

↓ mTORC1

Mitochondrial activity ↓

↓ Hemoglobin content

Erythroid precursor

Ter119

↓ Hemoglobin content

Size ↓

Mature red blood cell

Antonio Bouthelier, Lucía Fernández-Arroyo, Claudia Mesa-Ciller, ..., Francisco Sánchez-Madrid, Andrés A. Urrutia, Julián Aragonés

julian.aragones@uam.es

Highlights

Expression of SLC7A5/ SLC3A2 amino acid carrier in immature erythroid cells

Erythropoietin regulates SLC7A5/SLC3A2 expression

Loss of SLC7A5 reduces size, hemoglobin and mTORC1 activity of erythroid cells

SLC7A5 sustains CD71 expression and mitochondrial activity in circulating reticulocytes

CellPress
OPEN ACCESS

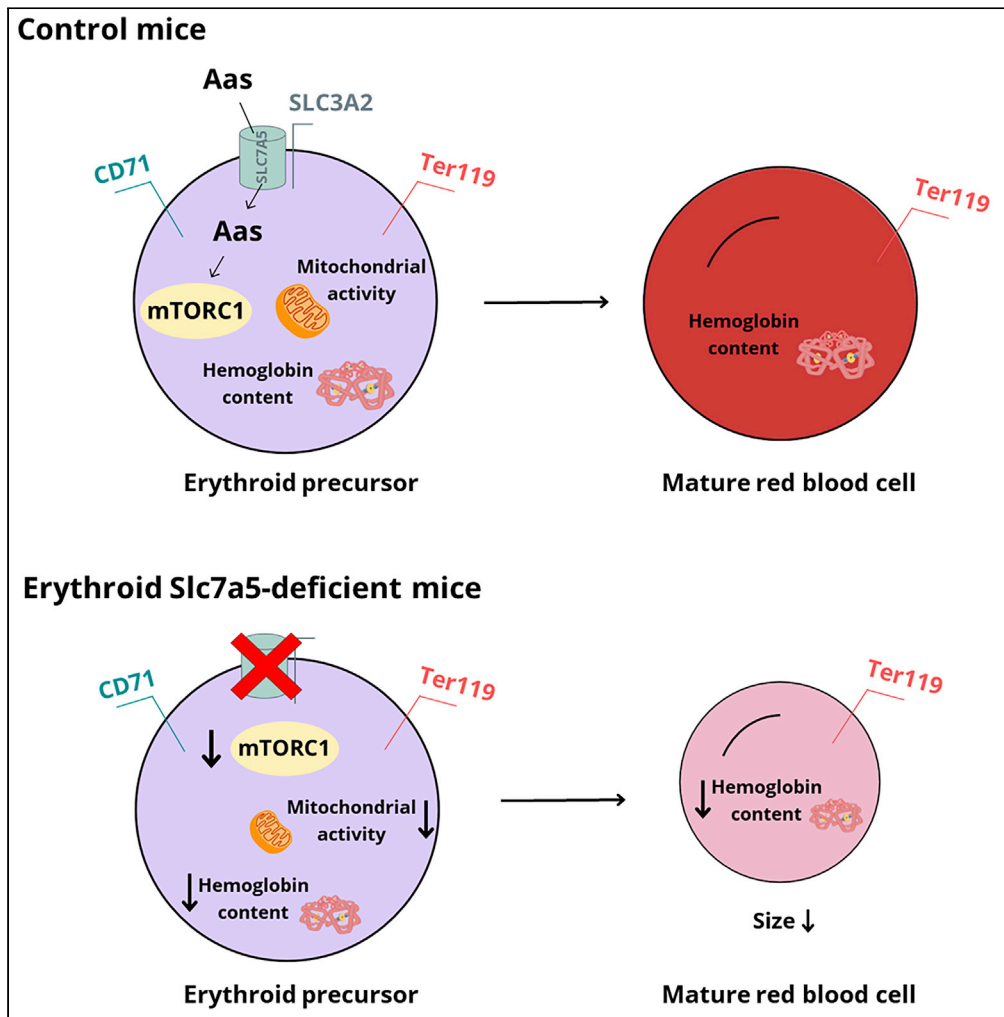## Article

Erythroid SLC7A5/SLC3A2 amino acid carrier controls red blood cell size and maturation

Antonio Bouthelier,[1,11] Lucía Fernández-Arroyo,[1,11] Claudia Mesa-Ciller,[1] Danay Cibrian,[2,8] Noa Beatriz Martín-Cófreces,[2,8] Raquel Castillo-González,[2,8,9] Macarena Calero,[3,4] Diego Herráez-Aguilar,[5] Andrea Guajardo-Grence,[1] Ana María Pacheco,[1] Ana Marcos-Jiménez,[2] Borja Quiroga,[6] Marta Morado,[7] Francisco Monroy,[3,4] Cecilia Muñoz-Calleja,[2] Francisco Sánchez-Madrid,[2,6,10] Andrés A. Urrutia,[1,12] and Julián Aragonés[1,10,12,13,*]

SUMMARY

Inhibition of the heterodimeric amino acid carrier SLC7A5/SLC3A2 (LAT1/CD98) has been widely studied in tumor biology but its role in physiological conditions remains largely unknown. Here we show that the SLC7A5/SLC3A2 heterodimer is constitutively present at different stages of erythroid differentiation but absent in mature erythrocytes. Administration of erythropoietin (EPO) further induces SLC7A5/SLC3A2 expression in circulating reticulocytes, as it also occurs in anemic conditions. Although *Slc7a5* gene inactivation in the erythrocyte lineage does not compromise the total number of circulating red blood cells (RBCs), their size and hemoglobin content are significantly reduced accompanied by a diminished erythroblast mTORC1 activity. Furthermore circulating *Slc7a5*-deficient reticulocytes are characterized by lower transferrin receptor (CD71) expression as well as mitochondrial activity, suggesting a premature transition to mature RBCs. These data reveal that SLC7A5/SLC3A2 ensures adequate maturation of reticulocytes as well as the proper size and hemoglobin content of circulating RBCs.

INTRODUCTION

Cells require specific transporters to take up different solutes, including amino acids. More than 400 different transporters have currently been identified and grouped into 60 families of Solute-Linked Carriers (SLCs) based on their structure.[1–3] Of these, 11 families are amino acid carriers that have been classified according to their substrate specificity and the participation of Na^+ ions in amino acid uptake.[4,5] The heterodimeric transporter SLC7A5/SLC3A2, composed of SLC7A5 (LAT1) light chain and a SLC3A2 (CD98hc or 4F2hc) heavy chain, is fundamental for the uptake of extracellular L-leucine, and ensuing the activation of the mammalian target of rapamycin (mTOR) pathway.[6–9] SLC7A5/SLC3A2-dependent mTORC1 activation has been largely explored in the context of tumor biology where it is essential to sustain tumor cell proliferation.[10–13] SLC7A5/SLC3A2 heterodimer also transports other large neutral amino acids including branched-chain amino acids (L-isoleucine and L-valine), aromatic amino acids (L-phenylalanine, L-tryptophan and L-tyrosine), L-histidine, L-methionine and L-glutamine.[14,15] Therefore, SLC7A5 is essential not only to activate mTORC1-dependent pathways but also, to promote mTORC1-independent pathways, as seen in tumor cells and activated immune cells.[13,16–20]

SLC7A5 is strongly expressed by endothelial cells that form the blood-brain barrier (BBB),[21,22] ensuring an essential supply of amino acids to brain tissue. In this line, *Slc7a5* gene inactivation in the endothelium of mice triggers a phenotype compatible with autism as well as delayed motor activity.[21,22] SLC3A2 is a type II multifunctional membrane glycoprotein with a transmembrane domain and a large N-terminal glycosylated ectodomain that stabilizes the SLC7A5 light chain on the plasma membrane.[15,23,24] In addition to SLC7A5, SLC3A2 can associate with other amino acid transporters including SLC7A8 (LAT2), SLC7A7 (y+LAT1), SLC7A6 (y+LAT2), SLC7A11 (xCT) and SLC7A10 (Asc-1). All of these are involved in the specific uptake of amino acids not transported by SLC7A5/SLC3A2, such as cysteine, alanine, or glutamate.[6,25–30]

[1]Research Unit, Hospital of Santa Cristina, Research Institute Princesa (IP), Autonomous University of Madrid, 28009 Madrid, Spain

[2]Immunology Department, Hospital de la Princesa, Instituto Investigación Sanitaria Princesa, Universidad Autónoma de Madrid, Madrid, Spain

[3]Departamento de Química Física, Universidad Complutense de Madrid, Ciudad Universitaria s/n, Madrid, Spain

[4]Translational Biophysics. Instituto de Investigación Sanitaria Hospital Doce de Octubre (Imas12), Madrid, Spain

[5]Facultad de Ciencias Experimentales, Universidad Francisco de Vitoria, Ctra. Pozuelo-Majadahonda Km 1,800, 28223, Pozuelo de Alarcón, Madrid, Spain

[6]Nephrology Department, Hospital de la Princesa, Instituto Investigación Sanitaria Princesa, Universidad Autónoma de Madrid, Madrid, Spain

[7]Hematology Department, Hospital Universitario La Paz, Madrid, Spain

[8]Department of Vascular Biology and Inflammation, Centro Nacional de Investigaciones Cardiovasculares (CNIC), Madrid, Spain

[9]Pathology Anatomy Department, Instituto de Investigación Sanitaria Hospital 12 de Octubre (imas12), Madrid, Spain

[10]CIBER de Enfermedades Cardiovasculares, Carlos III

Continued

Erythropoiesis is the biological process by which mature RBCs are generated through the differentiation of hematopoietic stem cells (HSCs).[31–34] HSCs cells can differentiate into myeloid precursors and then into megakaryocyte-erythroid progenitors, which then turn into erythroid BFU-E (burst-forming unit-erythroid) and CFU-E (colony-forming unit-erythroid) precursors.[35,36] Subsequently, CFU-E cells differentiate into proerythroblasts, and then successively, to basophilic, polychromatic, and orthochromatic erythroblasts.[37,38] To form erythrocytes, these orthochromatic cells expel their nuclei to become enucleated cells called reticulocytes. These reticulocytes still contain mitochondria, RNA and ribosomes, while protein synthesis is lost progressively during the final step of erythroid differentiation when reticulocytes are converted to mature erythrocytes, adopting a biconcave shape through extensive membrane remodeling.[17,39–42] Erythroid maturation is morphologically identical in human and mouse erythroid cells, as reflected by the similar patterns of surface proteins, cytoskeleton components and transcriptional regulators found when these cells have been compared.[43–45] However, there are some differences in terms of the size, lifespan and oxygen affinity between human and mouse erythroid cells.[44] Moreover, at the molecular level there are differences in the specific patterns of genes expressed by human and mouse cells at similar stages of erythroid differentiation.[43,44] The basal rate of erythropoiesis may increase when the oxygen supply is compromised acutely (hypoxia), provoking an erythropoietic stress response.[46,47] This response is initiated when oxygen supply to the kidneys is reduced, which activates the hypoxia-inducible factor 2α (HIF2α) and increases the transcription of the erythropoietin (Epo) gene, thereby elevating circulating EPO levels.[48–52] In adults, EPO is mainly produced by peritubular cells of the kidney, characterized by the expression of FOXD1, and to a lesser extent by hepatocytes.[50,52–55] EPO promotes the expansion of erythroid BFU-E and CFU-E precursors, acting through EPOR surface receptors that in turn activate signaling pathways, such as those involving STAT5, MAPK and/or PI3K/AKT via JAK2.[32,56–60]

The biological role of SLC7A5/SLC3A2 has been mainly explored in tumor cells although its physiological role remains largely unknown. Here we show that SLC7A5/SLC3A2 heterodimer is already expressed by early erythroid precursors being highest in more advanced stages of erythrocyte differentiation although its expression is finally lost in mature erythrocytes. Moreover, SLC7A5/SLC3A2 expression is further elevated by erythropoietic stress under anemic conditions, as well as following recombinant human EPO (rhEPO) administration. We also show that circulating RBCs of erythroid Slc7a5-deficient mice have reduced size and hemoglobin content in parallel to an attenuated mTORC1 activity in erythroblasts. Moreover erythroid Slc7a5 gene inactivation results in circulating reticulocytes with signs of premature transition to mature erythrocytes such as reduced CD71 transferrin receptor expression and lower mitochondrial membrane potential in circulating reticulocytes. Finally, this erythroid dysfunction upon Slc7a5 gene inactivation leads to compensatory hypererythropoietinemia.

RESULTS

Basal expression of the SLC7A5/SLC3A2 amino acid carrier in splenic erythrocyte precursors

To study the role of the SLC7A5/SLC3A2 (LAT1/CD98) amino acid carrier in biological scenarios other than proliferating tumor cells, we assessed whether the SLC7A5/SLC3A2 heterodimeric amino acid carrier might be expressed in the erythroid lineage, bearing in mind that sustained erythroblast proliferation is required to renew circulating RBCs.[61] To identify the different stages of erythrocyte differentiation we analyzed by flow cytometry the expression of specific cell surface markers, such as CD71 (transferrin receptor) and Ter119 (murine Glycophorin A).[37,38] Indeed, immature erythroblasts are characterized by high CD71 expression in conjunction with low or no Ter119 expression (CD71^{HI}/Ter119$^{NEG/LOW}$), whereas erythroblasts express both CD71 and Ter119 strongly at more advanced stages of erythroid maturation (CD71^{HI}/Ter119^{HI}) (Figure 1A). Moreover, fully differentiated erythrocytes are characterized by strong Ter119 expression and the absence of CD71 (CD71^{NEG}/Ter119^{HI}). Finally, there are also cells that do not express Ter119 together with very low or no expression of CD71 (CD71$^{NEG/LOW}$/Ter119^{NEG}), which includes splenic cells that do not belong to the erythroid lineage (Figure 1A).

Cell surface expression of SLC3A2 was found in immature splenic CD71^{HI}/Ter119$^{NEG/LOW}$ erythroblasts as well as by CD71^{HI}/Ter119^{HI} cells (Figures 1A and 1B). By contrast, SLC3A2 on the surface of splenic mature CD71^{NEG}/Ter119^{HI} erythrocytes was barely detected or absent (Figures 1A and 1B). We also found constitutive SLC3A2 surface expression in splenic CD71$^{NEG/LOW}$/Ter119^{NEG} cells, although more weakly than on CD71^{HI}/Ter119^{HI} double-positive erythroblasts (Figures 1A and 1B). There is not currently an antibody suitable to detect surface mouse SLC7A5 expression by flow cytometry. To ascertain whether this surface SLC3A2 expression can be attributed to the SLC7A5/SLC3A2 heterodimer, it should be considered that

Health Institute, Madrid, Spain

[11]These authors contributed equally

[12]These authors contributed equally

[13]Lead contact

*Correspondence: julian.aragones@uam.es

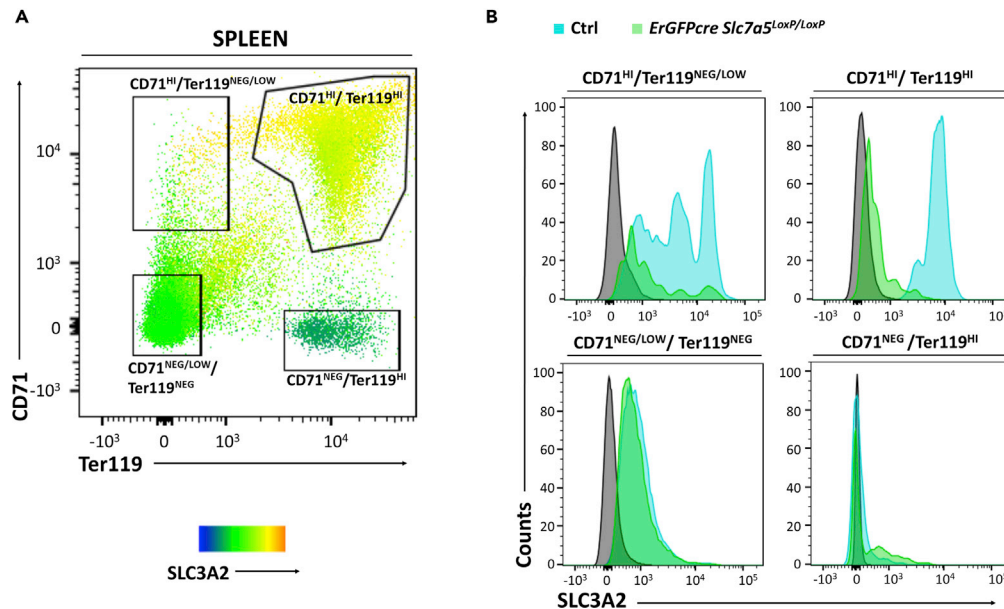https://doi.org/10.1016/j.isci.2022.105739

A

B

Figure 1. Basal expression of SLC7A5/SLC3A2 in the erythroid lineage

(A) The panel represents the flow cytometry analysis showing the different splenic cell populations in basal conditions based on the surface expression of CD71 and Ter119 in control mice. SLC3A2 expression is also represented by a color code: yellow-orange representing the strongest expression and dark green-blue the weakest or absence of expression.

(B) Histograms showing SLC3A2 expression in the different splenic CD71^HI/Ter119^NEG/LOW, CD71^HI/Ter119^HI, CD71^NEG/Ter119^HI and CD71^NEG/LOW/Ter119^NEG cell populations in control (in blue) and *ErGFPcre Slc7a5^LoxP/LoxP* mice (in green). The IgG control (in gray) is included. A representative experiment out of 23 is shown.

protein expression of SLC3A2 depends on the heterodimerization with SLC7A5.[10,62,63] Indeed, previous studies have shown that SLC7A5 gene inactivation leads to a remarkable suppression of SLC3A2 protein expression.[10,62,63] Therefore, to ascertain whether the surface SLC3A2 expression can be attributed to SLC7A5/SLC3A2 heterodimer, we generated *ErGFPcre Slc7a5^LoxP/LoxP* mice in which *Slc7a5* locus can be deleted specifically in the erythroid lineage. To achieve this, we crossed *Slc7a5^LoxP/LoxP* mice, in which a genomic region including the exon 1 of *Slc7a5* was flanked by two *LoxP* sites,[19] with *ErGFPcre* mice that express the Cre recombinase under the control of the EPOR promoter.[64] A PCR analysis using primers at 5′ position of the 5′ *LoxP* site and 3′ position of the 3′ *LoxP* site already used[19] amplifies a 253 bp band from DNA obtained from the spleen of *ErGFPcre Slc7a5^LoxP/LoxP* mice that was not amplified in control mice, indicating that exon 1 of *Slc7a5* was efficiently deleted in the *ErGFPcre Slc7a5^LoxP/LoxP* mice (Figure S1). In this line, basal splenic *Slc7a5* mRNA was lower in *ErGFPcre Slc7a5^LoxP/LoxP* mice (Figure 2B). Importantly, basal SLC3A2 flow cytometry signal was strongly reduced in splenic CD71^HI/Ter119^NEG/LOW erythroblasts, as well as in CD71^HI/Ter119^HI cells of *ErGFPcre Slc7a5^LoxP/LoxP* mice, whereas the SLC3A2 signal did not diminish in splenic CD71^NEG/LOW/Ter119^NEG cells (Figure 1B), consistent with the ability of *ErGFPcre* mice to specifically inactivate genes in the erythroid lineage. These data demonstrate that the SLC7A5/SLC3A2 heterodimer is specifically expressed at different stages of erythrocyte differentiation but markedly declined during the final step of this differentiation toward fully differentiated mature erythrocytes.

SLC7A5/SLC3A2 expression in splenic erythroblasts in anemic conditions

Erythroblasts proliferate rapidly in anemic conditions to restore appropriate numbers of circulating mature erythrocytes, as an erythropoietic stress response that largely relies on the erythropoietic potential of the spleen.[46,47,61] Therefore, we assessed SLC7A5/SLC3A2 expression in the spleen of control and *ErGFPcre Slc7a5^LoxP/LoxP* mice in anemic conditions. To study this we first induced anemia in mice by administering phenylhydrazine (PHZ), an oxidizing agent that provokes severe hemolysis. These anemic conditions led to a marked accumulation of splenic CD71^HI/Ter119^HI cells (Figure 2A). In comparison with baseline conditions, PHZ-treated control mice showed higher expression of splenic *Slc7a5* mRNA whereas its expression was remarkably lower in PHZ-treated *ErGFPcre Slc7a5^LoxP/LoxP* mice (Figure 2B). Along this line, immature splenic CD71^HI/Ter119^NEG/LOW erythroblasts and CD71^HI/Ter119^HI cells underwent a specific elevation of
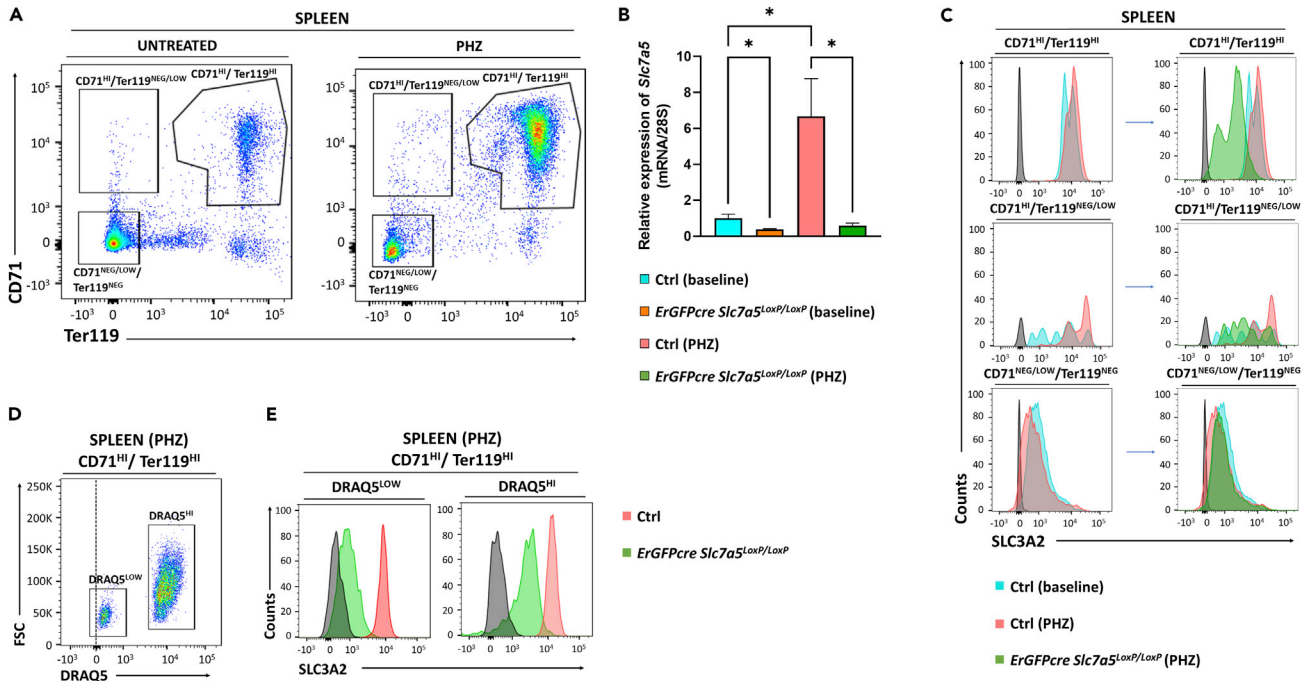
Figure 2. SLC7A5/SLC3A2 expression in splenic erythroblasts during erythropoietic stress

(A) Representative flow cytometry analysis showing the different splenic cell populations in control and PHZ-treated mice based on the surface expression of CD71 and Ter119: CD71^{HI}/Ter119$^{NEG/LOW}$, CD71^{HI}/Ter119^{HI}, and CD71$^{NEG/LOW}$/Ter119^{NEG}.

(B) Relative *Slc7a5* mRNA expression in the spleen of control (n = 8) and *ErGFPcre Slc7a5$^{LoxP/LoxP}$* (n = 3) mice in baseline conditions as well as control (n = 6) and *ErGFPcre Slc7a5$^{LoxP/LoxP}$* (n = 5) upon PHZ treatment. Data are shown as mean $\pm$ SEM. Statistical analysis was performed using a two-tailed Student's *t* test with Welch's correction to compare the groups as indicated in the figure (*p < 0.05).

(C) Histograms showing SLC3A2 expression in each of the populations indicated in untreated control mice (in blue) and control mice treated with PHZ (in red) are shown in left panels. In the right panels, the same histograms of the left panels are shown, but overlaying the histogram of SLC3A2 expression of *ErGFPcre Slc7a5$^{LoxP/LoxP}$* (in green) mice treated with PHZ. The IgG-APC control is presented in gray. For A and C a representative experiment out of 9 is shown.

(D) Representative flow cytometry analysis of DRAQ5 expression versus forward scatter (FSC) of the splenic CD71^{HI}/Ter119^{HI} erythroid population of PHZ-treated control mice. Two CD71^{HI}/Ter119^{HI} populations differing in DRAQ5 signal can be distinguished, DRAQ5^{HI} and DRAQ5^{LOW}. The dashed line represents unlabeled cells.

(E) Representative histograms of SLC3A2 expression in CD71^{HI}/Ter119^{HI}/DRAQ5^{HI} and CD71^{HI}/Ter119^{HI}/DRAQ5^{LOW} populations in control mice treated with PHZ (in red) and *ErGFPcre Slc7a5$^{LoxP/LoxP}$* (in green) mice treated with PHZ are shown. The negative signal of the IgG-PyC control is shown in gray. For D and E a representative experiment out of 7 is shown.

SLC3A2 surface expression (Figure 2C, upper and middle left panels) while SLC3A2 was not altered in CD71$^{NEG/LOW}$/Ter119^{NEG} non-erythroid splenic cells (Figure 2C, lower left panel). A parallel analysis in PHZ-treated *ErGFPcre Slc7a5$^{LoxP/LoxP}$* mice showed that - in contrast to baseline conditions (Figure 1B) - SLC3A2 surface expression was partially reduced in immature CD71^{HI}/Ter119$^{NEG/LOW}$ and CD71^{HI}/Ter119^{HI} erythroblasts when compared with PHZ-treated control mice (Figure 2C, upper and middle right panels), which might suggest that not only SLC7A5/SLC3A2 but also other amino acid carrier partners of SLC3A2 might be induced in CD71^{HI}/Ter119$^{NEG/LOW}$ and CD71^{HI}/Ter119^{HI} cells under conditions of erythropoietic stress. A more detailed analysis of the CD71^{HI}/Ter119^{HI} cells in PHZ-treated *ErGFPcre Slc7a5$^{LoxP/LoxP}$* mice identified a subpopulation of CD71^{HI}/Ter119^{HI} cells in which SLC3A2 expression was largely reduced and another in which SLC3A2 was only partially diminished when compared to PHZ-treated control mice (Figure 2C, upper right panel in CD71^{HI}/Ter119^{HI} cells).

CD71^{HI}/Ter119^{HI} cells are nucleated basophilic, polychromatic, orthochromatic erythroblasts as well as enucleated reticulocytes that only contain RNA.[37,65] Indeed, a further analysis of the DNA/RNA content of CD71^{HI}/Ter119^{HI} cells using the DNA/RNA fluorescent probe DRAQ5 indicated that the CD71^{HI}/Ter119^{HI} population in PHZ-treated mice was composed of a subpopulation of nucleated cells with a high DRAQ5 signal (DRAQ5^{HI}), and a second subpopulation of enucleated reticulocytes still having RNA molecules with

a low DRAQ5 signal (DRAQ5^{LOW}) (Figure 2D). CD71^{HI}/Ter119^{HI}/DRAQ5^{HI} nucleated cells showed a partial decline of surface SLC3A2 expression in *ErGFPcre Slc7a5$^{LoxP/LoxP}$* mice (Figure 2E), suggesting that nucleated CD71^{HI}/Ter119^{HI} cells in conditions of erythropoietic stress not only express SLC7A5/SLC3A2 but also other SLC3A2 partners. However, DRAQ5^{LOW} reticulocytes were the CD71^{HI}/Ter119^{HI} subpopulation in which surface SLC3A2 expression was more markedly diminished (Figure 2E), suggesting that SLC7A5 is the predominant partner of SLC3A2 in splenic reticulocytes.

SLC7A5/SLC3A2 in circulating reticulocytes involves erythropoietin signaling

We next assessed the surface expression of SLC3A2 in circulating cells. The vast majority of them were CD71^{NEG}/Ter119^{HI} mature erythrocytes in control mice, with a small proportion of CD71^{HI}/Ter119^{HI} cells. However, PHZ administration produced a remarkable increase in the proportion of circulating CD71^{HI}/Ter119^{HI} cells (Figure 3A), which are exclusively DRAQ5^{LOW} (Figure S2), indicating that they are reticulocytes released from the spleen during stress erythropoiesis. This increase in the proportion of circulating CD71^{HI}/Ter119^{HI} cells was also observed when anemic conditions were generated by subjecting mice to phlebotomy (Figure 3A). Therefore, and as observed in splenic reticulocytes, the basal SLC3A2 surface expression of CD71^{HI}/Ter119^{HI} reticulocytes was further increased in both anemic conditions (Figure 3B). Moreover, in circulating CD71^{HI}/Ter119^{HI} of PHZ-treated mice, SLC3A2 expression was strongly decreased in homozygous *ErGFPcre Slc7a5$^{LoxP/LoxP}$* and accordingly partially decreased in heterozygous *ErGFPcre Slc7a5$^{LoxP/+}$* (Figure 3B). Therefore, these data further suggest that SLC7A5 is the principal partner of SLC3A2 not only in splenic (Figure 2E) but also in circulating reticulocytes (Figure 3B). We further confirmed SLC7A5 protein expression in circulating erythroid cells of PHZ-treated control mice but was undetectable in PHZ-treated *ErGFPcre Slc7a5$^{LoxP/LoxP}$* mice (Figure 3C). Moreover, SLC7A5 carrier activity in circulating CD71^{HI}/Ter119^{HI} reticulocytes assessed by the uptake of L-phenylalanine was significantly reduced in circulating CD71^{HI}/Ter119^{HI} reticulocytes of *ErGFPcre Slc7a5$^{LoxP/LoxP}$* mice (Figure 3D). To evaluate the clinical value of our data, we also analyzed circulating reticulocytes in anemic subjects by assessing by flow cytometry the expression of CD71 and Glycophorin-A (GYPA or CD235a), the latter a surface marker homologous to Ter119 in mice. There was a limited proportion of circulating CD71^{HI}/GYPA^{HI} reticulocytes in the blood of control subjects, which increased markedly in anemic subjects (Figure 3E). In line with the data obtained in mice, SLC3A2 was specifically induced in circulating CD71^{HI}/GYPA^{HI} reticulocytes from anemic relative to control subjects while its expression was absent in mature circulating CD71^{NEG}/GYPA^{HI} erythrocytes in both healthy and anemic subjects (Figure 3E).

Since surface SLC7A5/SLC3A2 expression was elevated in two different models of anemia such as PHZ and phlebotomy, we asked whether this might be a consequence of elevated serum EPO levels in anemic conditions. Therefore, we asked whether EPO signaling might be involved in the induction of SLC7A5/SLC3A2 expression in the erythroid lineage. To assess this, we injected recombinant human EPO (rhEPO) into control mice and after two days, we found an increased expression of surface SLC3A2 expression in circulating CD71^{HI}/Ter119^{HI} cells (Figure 3F) as observed in anemic conditions. Moreover, this surface SLC3A2 surface expression was markedly reduced in *ErGFPcre Slc7a5$^{LoxP/LoxP}$* mice (Figure 3F). Therefore, the SLC7A5/SLC3A2 expression induced in circulating reticulocytes might be a consequence of an increase in EPO in response to anemic conditions.

Collectively, these data show that the SLC7A5/SLC3A2 heterodimer is expressed at different stages of erythrocyte differentiation but finally, it is lost in mature erythrocytes. Moreover, our data suggest that SLC7A5 is the predominant SLC3A2 subunit partner in splenic and circulating reticulocytes, with this SLC7A5/SLC3A2 heterodimer induced in response to erythropoietic stress, as well as in response to rhEPO administration.

Erythroid *Slc7a5*-deficient mice develop hypererythropoietinemia

Increased renal *Epo* gene expression and the ensuing elevation of circulating EPO levels are signs of insufficient tissue oxygenation in anemic conditions.[51,54] Therefore, we considered that - in case of dysfunctional erythropoiesis in *ErGFPcre Slc7a5$^{LoxP/LoxP}$* - the circulating EPO levels might be higher in *ErGFPcre Slc7a5$^{LoxP/LoxP}$* than in control mice. Indeed, in anemic conditions - upon PHZ or phlebotomy treatment - there was more serum EPO in *ErGFPcre Slc7a5$^{LoxP/LoxP}$* mice than in control mice (Figure 4A). Moreover, the induction of renal *Epo* mRNA was also stronger in *ErGFPcre Slc7a5$^{LoxP/LoxP}$* than in control mice under anemic conditions (Figure 4A). As shown above, SLC7A5/SLC3A2 is also expressed in erythroblasts under basal conditions (Figure 1A); we, therefore, assessed whether basal serum EPO levels were also elevated in
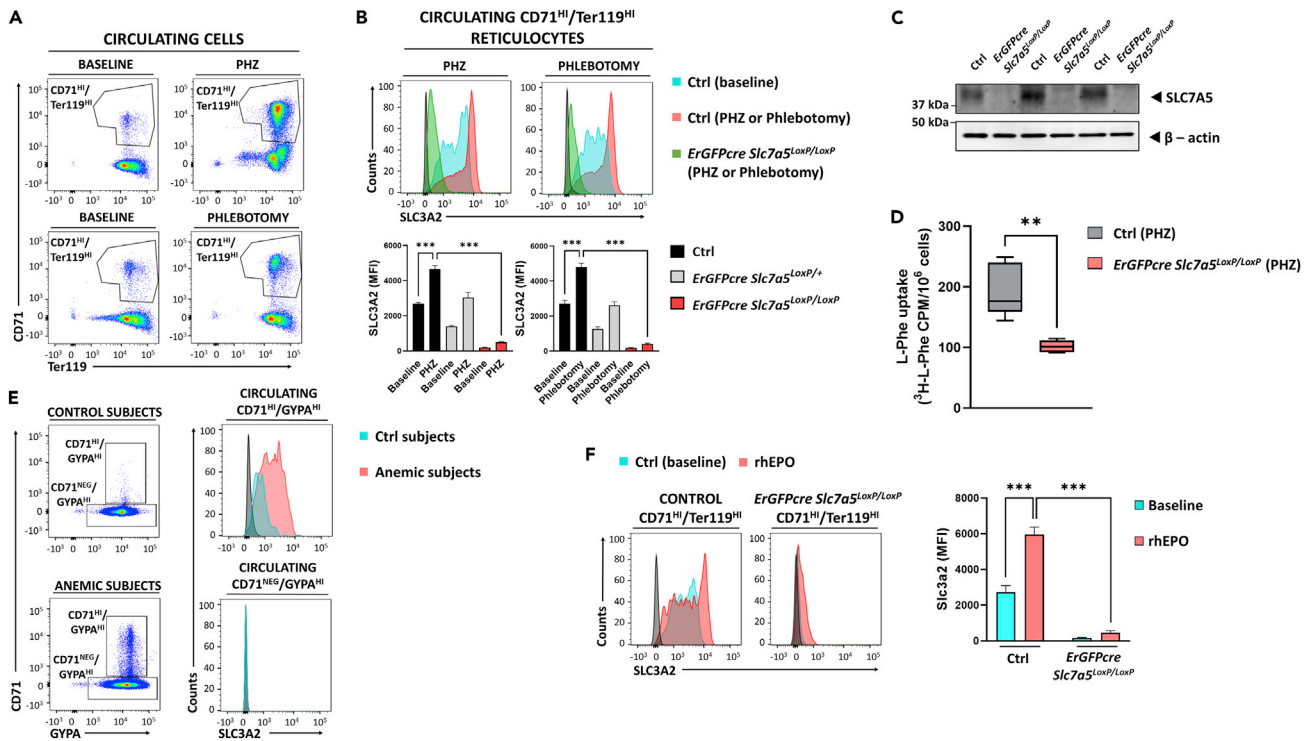
Figure 3. SLC7A5/SLC3A2 expression in circulating CD71^HI/Ter119^HI reticulocytes under anemic conditions and in response to rhEPO

(A) Representative flow cytometry analysis showing circulating CD71^HI/Ter119^HI reticulocytes in PHZ-treated and control mice, as well as in mice subjected to phlebotomy. For PHZ a representative experiment out of 20 is shown. For phlebotomy, a representative experiment out of 8 is shown.

(B) Representative histograms of SLC3A2 expression in circulating CD71^HI/Ter119^HI reticulocytes of untreated control mice (in blue), mice treated with PHZ or mice subjected to phlebotomy (in red), as well as *ErGFPcre Slc7a5^LoxP/LoxP* mice treated with PHZ or subjected to phlebotomy (in green). The IgG-APC control is represented in gray. Quantification of the mean fluorescence intensity (MFI) of SLC3A2 on circulating CD71^HI/Ter119^HI reticulocytes from control untreated mice (n = 33), control mice treated with PHZ (n = 20), *ErGFPcre Slc7a5^LoxP/+* untreated mice (n = 11), *ErGFPcre Slc7a5^LoxP/+* mice treated with PHZ (n = 10), *ErGFPcre Slc7a5^LoxP/LoxP* untreated mice (n = 16) and *ErGFPcre Slc7a5^LoxP/LoxP* mice treated with PHZ (n = 14). Quantification of the mean fluorescence intensity (MFI) of SLC3A2 on circulating CD71^HI/Ter119^HI reticulocytes from control mice (n = 8), control mice subjected to phlebotomy (n = 8), *ErGFPcre Slc7a5^LoxP/+* untreated mice (n = 4), *ErGFPcre Slc7a5^LoxP/+* mice subjected to phlebotomy (n = 4), *ErGFPcre Slc7a5^LoxP/LoxP* untreated mice (n = 3) and *ErGFPcre Slc7a5^LoxP/LoxP* mice subjected to phlebotomy (n = 3).

(C) Western blot analyses of SLC7A5 relative to β-actin protein levels in circulating erythroid cells of control and *ErGFPcre Slc7a5^LoxP/LoxP* PHZ-treated mice.

(D) L-phenylalanine uptake in isolated CD71^HI/Ter119^HI circulating reticulocytes from PHZ-treated control or *ErGFPcre Slc7a5^LoxP/LoxP* mice (n = 5).

(E) Representative flow cytometry analysis of CD71 expression versus GYPA in healthy and anemic subjects (left panels). Histograms of SLC3A2 expression in circulating CD71^HI/GYPA^HI and CD71^NEG/GYPA^HI populations of control (blue) and anemic (red) subjects (right panels). A representative experiment out of 3 anemic subjects and 3 control subjects is shown.

(F) Representative histograms of SLC3A2 expression in circulating CD71^HI/Ter119^HI reticulocytes of untreated control mice (blue) or mice treated with rhEPO (200U) (red). The IgG-APC control is represented in gray. Quantification of the mean fluorescence intensity (MFI) of SLC3A2 on circulating CD71^HI/Ter119^HI reticulocytes from untreated (n = 5) or rhEPO-treated control mice (n = 5), as well as from untreated (n = 3) or rhEPO-treated *ErGFPcre Slc7a5^LoxP/LoxP* mice (n = 5).

Data are shown as mean ± SEM. Statistical analysis was performed using one-way ANOVA followed by Tukey's post hoc test when comparing more than two groups or two-tailed Student's t test with Welch's correction when comparing two groups (**$p < 0.01$; ***$p < 0.005$).

ErGFPcre Slc7a5^LoxP/LoxP mice. Indeed, we also found higher basal serum EPO in *ErGFPcre Slc7a5^LoxP/LoxP* mice (Figure 4A). Notably, circulating EPO or *Epo* mRNA induction was not significantly altered in heterozygous *ErGFPcre Slc7a5^LoxP/+* mice (Figure 4A), demonstrating that the inactivation of both *Slc7a5* alleles is required to develop this hypererythropoietinemia found in *ErGFPcre Slc7a5^LoxP/LoxP* mice. Thus, we reasoned that an erythroid SLC7A5 deficiency might affect the number of circulating RBCs, potentially explaining this hypererythropoietinemia. However, the number of circulating RBCs was not reduced in *ErGFPcre Slc7a5^LoxP/LoxP* mice under basal conditions or under anemic conditions after PHZ administration (Figure 4B). In addition, we did not find significant differences in serum LDH activity (809.3 ± 110.7 U/L in control mice (n = 7) vs. 991.6 ± 168.1 U/L in erythroid *Slc7a5*-deficient mice (n = 5), P=NS, non-significant) suggesting that RBCs of *ErGFPcre Slc7a5^LoxP/LoxP* mice did not show signs of hemolysis. Therefore, the
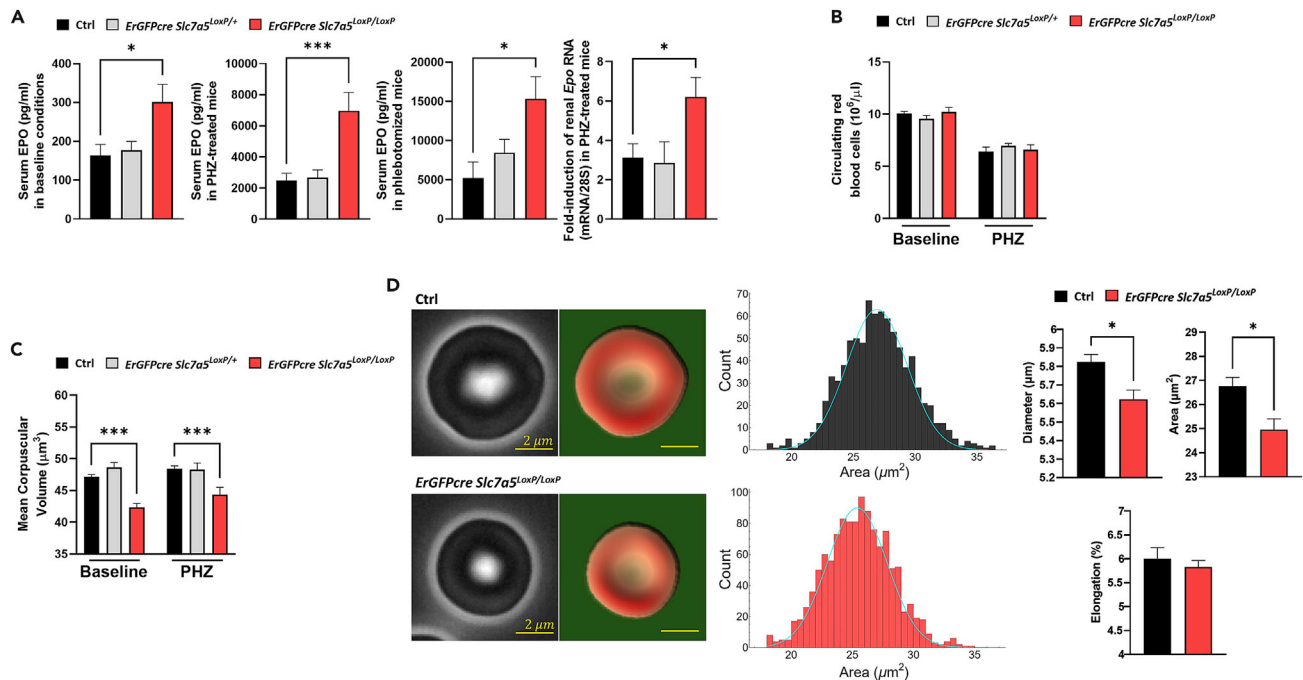
Figure 4. Mice lacking SLC7A5 in the erythroid lineage develop hypererythropoietinemia and smaller circulating RBCs

(A) Serum EPO protein (pg/mL) in control mice (n = 18), *ErGFPcre Slc7a5*^{LoxP/+} mice (n = 4), and *ErGFPcre Slc7a5*^{LoxP/LoxP} mice (n = 13) under baseline conditions; in control mice (n = 18), *ErGFPcre Slc7a5*^{LoxP/+} mice (n = 9) and *ErGFPcre Slc7a5*^{LoxP/LoxP} mice (n = 16) after PHZ treatment; and in phlebotomized control mice (n = 6), *ErGFPcre Slc7a5*^{LoxP/+} mice (n = 4) and *ErGFPcre Slc7a5*^{LoxP/LoxP} mice (n = 6).

(B) Total number of circulating RBCs in control mice (n = 28), *ErGFPcre Slc7a5*^{LoxP/+} mice (n = 13), and *ErGFPcre Slc7a5*^{LoxP/LoxP} mice (n = 18) under basal conditions or in control mice (n = 13), *ErGFPcre Slc7a5*^{LoxP/+} mice (n = 9), and *ErGFPcre Slc7a5*^{LoxP/LoxP} mice (n = 13) after PHZ treatment.

(C) Mean corpuscular volume (MCV, μm³) of circulating RBCs in control mice (n = 28), *ErGFPcre Slc7a5*^{LoxP/+} mice (n = 13), and *ErGFPcre Slc7a5*^{LoxP/LoxP} mice (n = 18) under basal conditions, and in control mice (n = 11), *ErGFPcre Slc7a5*^{LoxP/+} mice (n = 7), and *ErGFPcre Slc7a5*^{LoxP/LoxP} mice (n = 12) after PHZ treatment.

(D) Representative images of life imaging morphology cytometry (left) and 3D-cell rendering images (right) of RBCs of *ErGFPcre Slc7a5*^{LoxP/LoxP} and control mice. The RBC populations normally distributed their areas around a central average smaller for the *ErGFPcre Slc7a5*^{LoxP/LoxP} specimens than for control mice (central panels). Graph panels show the diameter (μm), area (μm²), and elongation (%) of RBCs in control, and *ErGFPcre Slc7a5*^{LoxP/LoxP} mice. Data are shown as mean ± SEM. Statistical analysis was performed using one-way ANOVA followed by Tukey's post hoc test when comparing three groups or two-tailed Student's *t* test with Welch's correction when comparing two groups (*p < 0.05; ***p < 0.005).

hypererythropoietinemia in *ErGFPcre Slc7a5*^{LoxP/LoxP} mice cannot be attributed to significant differences in the number of circulating RBCs relative to control mice.

SLC7A5 regulates red blood cell size and hemoglobin content

We next ascertained whether some specific features of circulating RBCs might be altered in *ErGFPcre Slc7a5*^{LoxP/LoxP} mice, which could explain their hypererythropoietinemia. Indeed, the mean corpuscular volume (MCV) of circulating RBCs was significantly lower in *ErGFPcre Slc7a5*^{LoxP/LoxP} mice already in baseline conditions (Figure 4C). Furthermore, life imaging morphology cytometry (LIMC) revealed that the red blood cell area and diameter were significantly reduced in *ErGFPcre Slc7a5*^{LoxP/LoxP} mice while their elongation was not significantly reduced (Figure 4D). In line with these data, *ErGFPcre Slc7a5*^{LoxP/LoxP} mice showed a lower hematocrit value (Table S1), which can be attributed to the smaller size of their circulating RBCs and not to a reduction in their total number.

We also found that the mean corpuscular hemoglobin (MCH) was significantly lower in *ErGFPcre Slc7a5*^{LoxP/LoxP} mice and already manifested at baseline conditions as in the case of MCV values (Figure 5A). Furthermore, May-Grünwald-Giemsa staining also showed that SLC7A5/SLC3A2-deficient mature red blood cells have signs of hypochromia (Figure 5B), which is in agreement with the reduced values of MCH found in *ErGFPcre Slc7a5*^{LoxP/LoxP} mice. In agreement with these data *ErGFPcre Slc7a5*^{LoxP/LoxP} mice showed lower hemoglobin in the blood (Table S1). As mentioned above, the heterodimeric transporter SLC7A5/SLC3A2 is essential for the uptake of
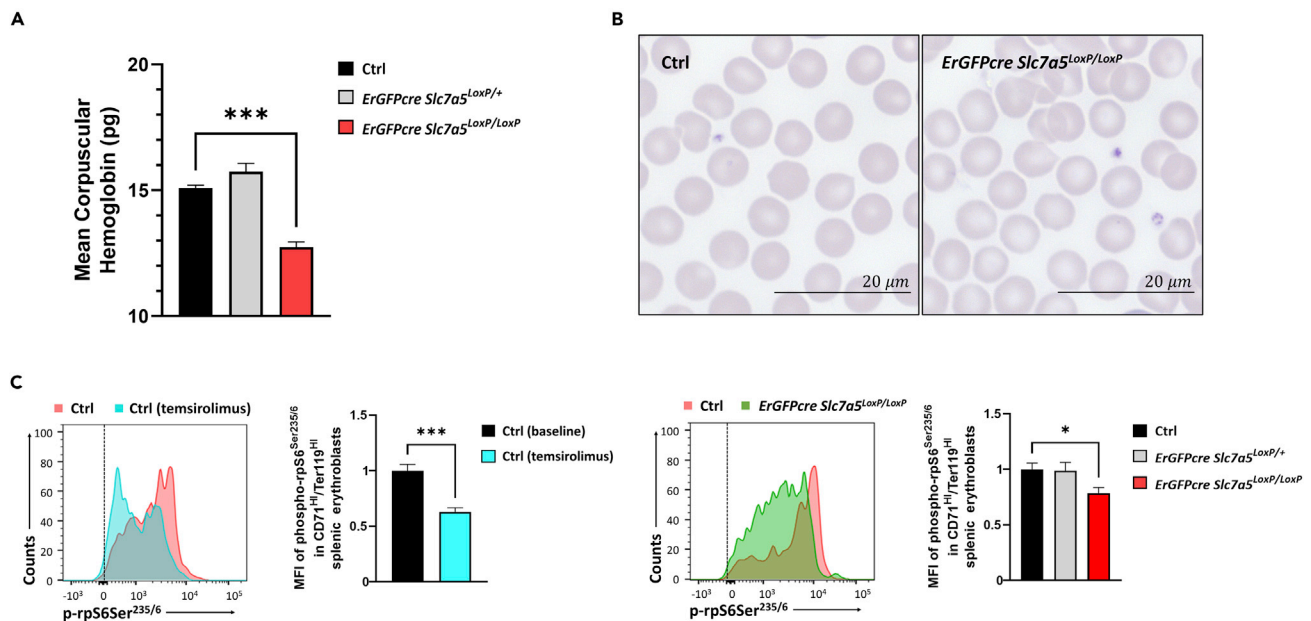
Figure 5. Erythroid-SLC7A5 deficient mice have red blood cells with lower hemoglobin content

(A) Mean corpuscular hemoglobin (MCH, pg) of circulating RBCs in control mice (n = 28), *ErGFPcre Slc7a5*[LoxP/+] mice (n = 13), and *ErGFPcre Slc7a5*[LoxP/LoxP] mice (n = 18) under basal conditions.

(B) Representative peripheral blood stainings with May-Grünwald-Giemsa of *ErGFPcre Slc7a5*[LoxP/LoxP] (right) and control (left) mice.

(C) Representative flow cytometry histograms comparing the phospho-rpS6[Ser235/6] signal in CD71[HI]/Ter119[HI] splenic erythroblasts of control and temsirolimus-treated mice (left panel). Representative flow cytometry histogram comparing the phospho-rpS6[Ser235/6] signal in CD71[HI]/Ter119[HI] splenic erythroblasts in control, and *ErGFPcre Slc7a5*[LoxP/LoxP] mice (right panel). Quantification of phospho-rpS6[Ser235/6] signal from control (n = 6) and temsirolimus-treated mice (n = 5) (left panel). Quantification of phospho-rpS6[Ser235/6] signal from control (n = 9), *ErGFPcre Slc7a5*[LoxP/+] mice (n = 8), and *ErGFPcre Slc7a5*[LoxP/LoxP] mice (n = 7) (right panel). The dashed line represents unlabeled permeabilized cells. Data are shown as mean ± SEM. Statistical analysis was performed using one-way ANOVA followed by Tukey's post hoc test when comparing three groups or two-tailed Student's *t* test with Welch's correction when comparing two groups (*p < 0.05; ***p < 0.005).

extracellular L-leucine, which leads to the activation of the central regulator of protein translation, the mammalian target of rapamycin (mTOR).[6,8] Therefore we considered whether reduced hemoglobin content in *Slc7a5*-deficient red blood cells might be associated a reduced mTORC1 activity, which has been shown to control erythroid hemoglobin translation.[66] For this purpose, we evaluated by flow cytometry the mTORC1 activity in erythroblasts assessing the phosphorylated form of the ribosomal protein S6 (rpS6) as a mTORC1 activation marker.[16,67] We first validated a phospho-rpS6[Ser235/6] signal in CD71[HI]/Ter119[HI] erythroblasts in control mice that were inhibited by treatment with the mTORC1 inhibitor, temsirolimus (Figure 5C). Importantly CD71[HI]/Ter119[HI] erythroblasts from *ErGFPcre Slc7a5*[LoxP/LoxP] mice showed lower levels of phospho-rpS6[Ser235/6] signal when compared with control or heterozygous *ErGFPcre Slc7a5*[LoxP/+] mice (Figure 5C). Therefore reduced erythroblastic mTORC1 activity provides a molecular explanation for the reduced hemoglobin content in red blood cells of erythroid *Slc7a5*-deficient mice.

Reduced CD71 expression and mitochondrial activity in SLC7A5 deficient red blood cells

While *ErGFPcre Slc7a5*[LoxP/LoxP] mice had a similar number of circulating RBCs (Figure 4B), a more detailed analysis revealed that they had fewer circulating CD71[HI]/Ter119[HI] reticulocytes with a simultaneous increase of cells with intermedium CD71 expression CD71[INT]/Ter119[HI] (Figure 6A). These CD71[INT]/Ter119[HI] cells have been previously shown to be in transition to mature erythrocytes.[17,39–42] Furthermore, we also observed an increased proportion of mature CD71[NEG]/Ter119[HI] erythrocytes (Figure 6A), which are cells that have lost their protein synthesis potential.[39] The transition of reticulocytes to mature erythrocytes is driven by a progressive clearance of mitochondria as a consequence of increased mitophagy, which is triggered by the inhibition of mTORC1 and the subsequent activation of the UNC51-like kinase-1 (ULK1).[17,40] Indeed, the loss of Ulk-1-dependent mitophagy prevents the conversion of reticulocytes to mature erythrocytes,[17,40] suggesting that mitochondrial clearance drives this conversion. Therefore, we assessed whether circulating CD71[HI]/Ter119[HI] reticulocytes in *ErGFPcre Slc7a5*[LoxP/LoxP] mice had a reduced
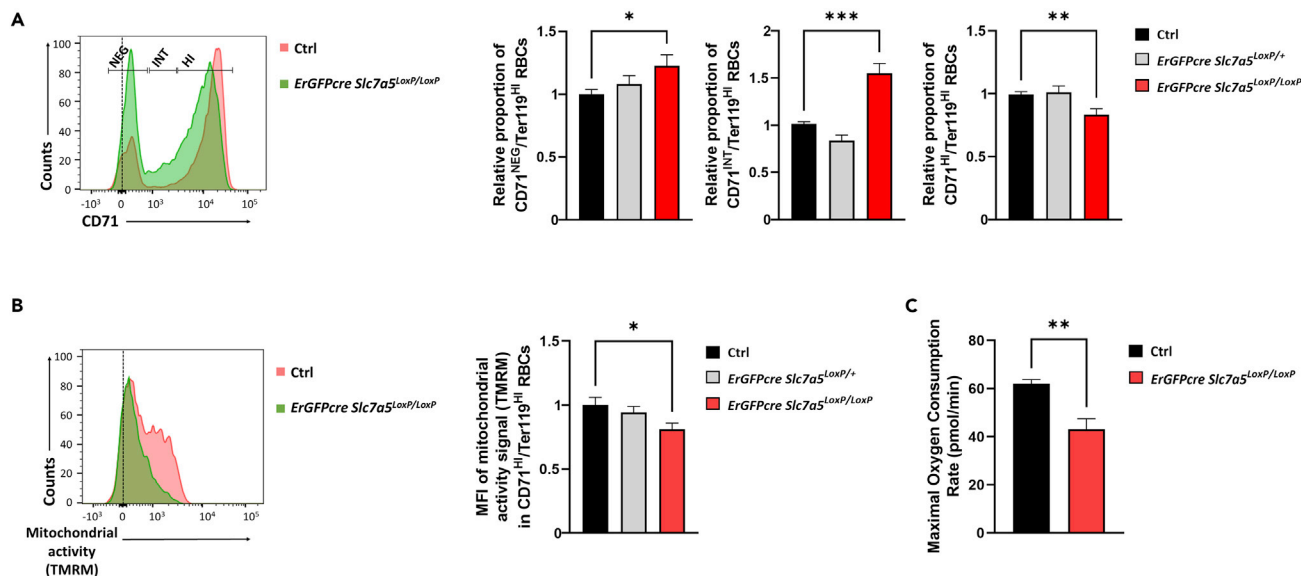
Figure 6. Loss of SLC7A5 in the erythroid lineage increases the transition between circulating reticulocytes and mature erythrocytes

(A) Flow cytometry histogram comparing the CD71 expressed by circulating Ter119 positive cells in a control, and *ErGFPcre Slc7a5^LoxP/LoxP* mice after PHZ treatment. Quantification of the proportion of CD71^HI/Ter119^HI, CD71^INT/Ter119^HI, and CD71^NEG/Ter119^HI in control (n = 35), *ErGFPcre Slc7a5^LoxP/+* mice (n = 19), and *ErGFPcre Slc7a5^LoxP/LoxP* mice (n = 28) after PHZ treatment. The range of CD71 expression considered for the quantification of CD71^HI/Ter119^HI, CD71^INT/Ter119^HI, and CD71^NEG/Ter119^HI RBCs is indicated.

(B) Flow cytometry histogram comparing the TMRM signal in circulating CD71^HI/Ter119^HI reticulocytes of control, and *ErGFPcre Slc7a5^LoxP/LoxP* mice after PHZ treatment. Quantification of TMRM signal from control (n = 7), *ErGFPcre Slc7a5^LoxP/+* mice (n = 6), and *ErGFPcre Slc7a5^LoxP/LoxP* mice (n = 7) after PHZ treatment. The dashed line represents unlabeled cells.

(C) Maximal mitochondrial oxygen consumption rate (OCR) in circulating cells of PHZ-treated mice (n = 14) and PHZ-treated *ErGFPcre Slc7a5^LoxP/LoxP* mice (n = 15).

Data are shown as mean ± SEM. Statistical analysis was performed using one-way ANOVA followed by Tukey's post hoc test when comparing three groups or two-tailed Student's t test with Welch's correction when comparing two groups (*p < 0.05; **p < 0.01; ***p < 0.005).

mitochondrial activity, which might accelerate their transition from CD71^HI/Ter119^HI reticulocytes to mature CD71^NEG/Ter119^HI erythrocytes. We evaluated the mitochondrial activity of circulating CD71^HI/Ter119^HI reticulocytes from *ErGFPcre Slc7a5^LoxP/LoxP* and control mice using tetramethylrhodamine methyl ester perchlorate (TMRM), which measures mitochondrial membrane potential as a surrogate marker of mitochondrial activity.[65,68] Control mice show TMRM signal in circulating CD71^HI/Ter119^HI reticulocytes (Figure 6B). Interestingly circulating CD71^HI/Ter119^HI reticulocytes had weaker mitochondrial potential signal in *ErGFPcre Slc7a5^LoxP/LoxP* mice (Figure 6B). In addition, we also stained cells with MitoTracker Green, a green-fluorescent dye that selectively accumulates in the mitochondria independently of mitochondrial potential. Similar to the TMRM signal, we found a lower MitoTracker Green signal in CD71^HI/Ter119^HI reticulocytes from *ErGFPcre Slc7a5^LoxP/LoxP* mice (Figure S3A). These data suggest that reduced mitochondrial activity in CD71^HI/Ter119^HI reticulocytes from *ErGFPcre Slc7a5^LoxP/LoxP* mice can be attributed to a lower mitochondrial content. Furthermore, we also confirmed that mitochondrial oxygen consumption was reduced upon *Slc7a5* gene inactivation in circulating erythroid cells in *ErGFPcre Slc7a5^LoxP/LoxP* mice (Figure 6C). Finally, mTORC1 inhibition with temsirolimus also reduced TMRM signal CD71^HI/Ter119^HI reticulocytes as well as the proportion of circulating CD71^HI/Ter119^HI reticulocytes (Figures S3B and S3C). Collectively these data suggest that mitochondrial dysfunction in CD71^HI/Ter119^HI reticulocytes lacking SLC7A5 expression as a consequence of reduced mTORC1 activity might be associated with premature transition of circulating reticulocytes toward mature erythrocytes.

Together the data presented here reveal the role of the SLC7A5/SLC3A2 amino acid carrier, which not only ensures the correct size and hemoglobin content of circulating RBCs but also regulates the maturation features of circulating reticulocytes such as reduced CD71 expression and mitochondrial activity.

DISCUSSION

The pathophysiological role of key amino acid carriers such as SLC7A5/SLC3A2 (LAT1/CD98) *in vivo* has raised great interest, especially in tumor biology and inflammatory diseases. Indeed, SLC7A5/SLC3A2 potentiates cell autonomous proliferation of tumor cells by regulating the uptake of key amino acids that are essential for mTORC1 activity, as well as for the translation of key pro-proliferative transcription factors such as c-Myc.[7,8,11,13,69] Moreover, SLC7A5/SLC3A2 is also fundamental for T lymphocyte and NK cell activation, involving mTORC1-dependent and independent mechanism.[16–18,20] However, the role of this amino acid carrier in basal physiological conditions in adults remains poorly understood. In these conditions, SLC7A5 was seen to be constitutively expressed in the endothelium of the BBB where it controls the amino acid supply to the brain parenchyma.[22] It was also shown to sustain mTORC1 activity and insulin sensitivity in skeletal muscle.[19]

Here we evaluated the role of SLC7A5/SLC3A2 in erythrocytes, considering that erythroblasts presumably require adequate amino acid supplies during erythropoiesis to maintain healthy circulating RBCs. SLC7A5/SLC3A2 is expressed by CD71^HI/Ter119^NEG/LOW early progenitors as well as by CD71^HI/Ter119^HI cells in baseline and anemic conditions contributing to amino acid uptake and mTORC1 activity in red blood cells. Strikingly erythroid-*Slc7a5* deficient mice did not show lower number of circulating RBCs in none of these two conditions . However, it should be considered that strong expression of SLC7A5/SLC3A2 is observed in those stages - including CD71^HI/Ter119^HI cells - in which hemoglobin is synthesized actively, even by reticulocytes.[39,70] Along this line, we found that erythrocyte *Slc7a5*-deficient mice had less hemoglobin in the blood, lower mean corpuscular hemoglobin and the presence of circulating hypochromic erythrocytes, suggesting that SLC7A5/SLC3A2 is essential for adequate cellular amino acid carrier activity required for hemoglobin biosynthesis, a phenomenon that cannot be fully compensated by other amino acid carriers. Our data also suggest that the reduced hemoglobin content in erythroid *Slc7a5*-deficient mice can be attributed to their diminished mTORC1 activity. In this line, it has been previously shown that mTORC1 firstly regulates the translation of the erythroid *Hba-a1* and *Hbb-b1* transcripts, which encode α- and β-globin respectively, the protein subunits of hemoglobin.[66] Moreover, the expression of SLC7A5/SLC3A2 mirrors the expression of the CD71 transferrin receptor in CD71^HI/Ter119^HI cells, suggesting that amino acid and iron loading needs to be coupled for hemoglobin synthesis.

SLC7A5/SLC3A2 expression in erythroblasts is not only present in basal conditions but it is also induced in splenic erythroid precursors in anemic conditions during erythropoietic stress. A more detailed analysis showed that CD71^HI/Ter119^HI erythroblasts are nucleated (DRAQ5^HI) cells in which surface SLC3A2 expression is partially inhibited in *Slc7a5*-deficient mice. These data suggest that other amino acid carriers that heterodimerize with SLC3A2 might be also expressed in nucleated CD71^HI/Ter119^HI cells, which in principle are composed of basophilic, polychromatic, and orthochromatic erythroblasts.[37,38] By contrast, SLC3A2 expression is markedly reduced in CD71^HI/Ter119^HI/DRAQ5^LOW enucleated reticulocytes in erythroid *Slc7a5*-deficient mice, suggesting that SLC7A5/SLC3A2 is the predominant partner of SLC3A2 in splenic reticulocytes. CD71^HI/Ter119^HI reticulocytes but not CD71^HI/Ter119^HI nucleated erythroblasts exit the spleen to enter circulation[71,72] and hence, the predominant expression of SLC7A5 partnering SLC3A2 was also found in circulating reticulocytes. In terms of the increased expression of SLC7A5/SLC3A2 during erythroid differentiation, we found that EPO administration is sufficient to induce SLC7A5/SLC3A2 in circulating reticulocytes. These data suggest that EPOR activation in early erythroblast precursors during erythropoietic stress can act as an initial trigger for the sustained and elevated surface expression of SLC7A5/SLC3A2 from early CD71^HI/Ter119^NEG/LOW to CD71^HI/Ter119^HI circulating enucleated reticulocytes.

Our data show that - although RBCs are smaller and with low hemoglobin content - their number in circulation is not altered in erythroid *Slc7a5*-deficient mice. This might be surprising taking into consideration the influence of SLC7A5 on the tumor cell proliferation.[11,13,73,74] However, it is conceivable that the presence of other amino acid carriers that heterodimerize with SLC3A2 in CD71^HI/Ter119^HI nucleated erythroblasts might be enough to sustain the proliferation of these cells. In this line, we found evidence that other SLC3A2-dependent heterodimers - aside SLC7A5/SLC3A2 - seem to be expressed in CD71^HI/Ter119^HI nucleated cells, which might still be competent to drive the normal proliferation of these cells. Moreover, it should be considered more central participation of other types of amino acid carriers in erythroblasts proliferation such as CAT1 because its global inactivation leads to severe anemia.[75] Finally, we cannot rule out that a modest defect in erythroblast proliferation following *Slc7a5* gene inactivation compensated by an

increase in circulating EPO, which reinvigorates erythroid precursor proliferation resulting in a normalization of the number of circulating erythroid cells. In contrast to nucleated erythroblasts, SLC7A5 is the main partner of SLC3A2 in enucleated reticulocytes, and therefore, the absence of SLC7A5 is sufficient to elicit a reduction in their cell size and hemoglobin content that cannot be compensated by other SLC3A2-based amino acid carriers.

Our data also show that SLC7A5/SLC3A2 not only controls the correct size and hemoglobinization of circulating RBCs but also seems to regulate the transition of circulating reticulocytes to mature erythrocytes. Indeed, erythroid-specific *Slc7a5* gene inactivation decreases the proportion of circulating CD71^{HI}/Ter119^{HI} reticulocytes paralleled by an increase of circulating CD71^{INT}/Ter119^{HI} cells characterized by a weaker CD71 expression. In line with these data, an increased proportion of mature CD71^{NEG}/Ter119^{HI} erythrocytes was also observed. These data suggest that SLC7A5 prevents the premature transition of CD71^{HI}/Ter119^{HI} reticulocytes toward mature erythrocytes. Previous studies showed that weaker CD71 expression is a sign of reduced mitochondrial activity in reticulocytes.[76] Moreover, Ulk-1-dependent mitophagy and the ensuing mitochondrial clearance play a role in the transition of mature reticulocytes to mature erythrocytes.[17,40] Indeed, we show that SLC7A5-deficient CD71^{HI}/Ter119^{HI} reticulocytes have a reduced mitochondrial activity and maximal oxygen consumption that can be attributed to their reduced mitochondrial content. Hence, our data suggest that SLC7A5 expression in reticulocytes prevents the premature transition of CD71^{HI}/Ter119^{HI} reticulocytes toward mature erythrocytes by controlling mitochondrial clearance and surface expression of the CD71 transferrin receptor. This premature differentiation of reticulocytes might also be linked to reduced hemoglobin content, particularly taking into consideration that reticulocytes are characterized by a high rate of hemoglobin synthesis that is progressively lost as they become mature erythrocytes.[39] Furthermore, we also show that mTORC1 inhibition leads to reduced mitochondria activity in circulating CD71^{HI}/Ter119^{HI} reticulocytes as well as their proportion relative to mature cells. In this line, it should be considered that mitochondrial clearance is favored by reduced mTORC1 activity and subsequent Ulk-1 activation,[17,40] suggesting that the reduced mitochondrial activity and increased cells in transition from reticulocyte to mature erythrocyte in erythroid *Slc7a5*-deficient mice might be attributed to the reduced mTORC1 activity.

In summary, the data presented here reveal the physiological role of the SLC7A5/SLC3A2 amino acid carrier in the control of erythropoiesis, specifically controlling erythroblast size and hemoglobinization and the transition from circulating reticulocytes to mature erythrocytes.

Limitations of the study
As mentioned above the number of circulating RBCs is not altered upon *Slc7a5* gene inactivation in erythroid lineage, which might be surprising taking into consideration the influence of SLC7A5 on the tumor cell proliferation. However, RBCs in these erythroid *Slc7a5*-deficient mice are smaller with less hemoglobin thereby triggering compensatory hypererythropoietinemia most likely as a consequence of systemic hypoxia. Therefore, we cannot rule out that a potential defect in erythroblast proliferation following *Slc7a5* gene inactivation can be compensated by an increase in circulating EPO that reinvigorates erythroid precursor proliferation, normalizing the number of circulating erythroid cells.

STAR★METHODS
Detailed methods are provided in the online version of this paper and include the following:

- KEY RESOURCES TABLE
- RESOURCE AVAILABILITY
  - Lead contact
  - Materials availability
  - Data and code availability
- EXPERIMENTAL MODEL AND SUBJECT DETAILS
  - Mouse models
  - Patient samples
- METHOD DETAILS
  - RT-PCR, PCR analysis and primers
  - Phenylhydrazine (PHZ) treatment, phlebotomy, rhEPO administration and temsirolimus treatment
  - Hematological analysis

- ○ Life imaging morphology cytometry (LIMC)
- ○ Amino acid uptake assay
- ○ Oxygen consumption measurements
- ○ Flow cytometry
- ○ Serum EPO measurement
- ○ Western blot analysis
- ● QUANTIFICATION AND STATISTICAL ANALYSIS

SUPPLEMENTAL INFORMATION

Supplemental information can be found online at https://doi.org/10.1016/j.isci.2022.105739.

AUTHOR CONTRIBUTIONS

A.B. and L.F-A conducted most of the experiments. A.B., L.F-A, A.A.U., F.S.M, and J.A. were involved in the design of the experiments, data analysis, and writing of the article. L.F-A, R.C-G, D.C, A.M.P, and A.M-J. were involved in the flow cytometry analysis in mouse samples. L.F-A and A.B. were involved in RNA analysis. C.M.Ci., F.M., D.H-A., and M.C. were involved in the hematological as well as area and cell diameter analysis. M.M was involved in the May-Grünwald-Giemza staining. D.C. was involved in amino acid uptake analysis. N. M—C was involved in oxygen consumption measurements. A.M-J and C.M—Ca were involved in the flow cytometry analysis in anemic and healthy subjects. B.Q. was involved in the rhEPO administration experiments in mice.

DECLARATION OF INTERESTS

The authors declare no competing interests.

REFERENCES

1. Höglund, P.J., Nordström, K.J.V., Schiöth, H.B., and Fredriksson, R. (2011). The solute carrier families have a remarkably long evolutionary history with the majority of the human families present before divergence of bilaterian species. Mol. Biol. Evol. *28*, 1531–1541.

2. Perland, E., and Fredriksson, R. (2017). Classification Systems of secondary active transporters. Trends Pharmacol. Sci. *38*, 305–315.

3. Schumann, T., König, J., Henke, C., Willmes, D.M., Bornstein, S.R., Jordan, J., Fromm, M.F., and Birkenfeld, A.L. (2020). Solute carrier transporters as potential targets for the treatment of metabolic disease. Pharmacol. Rev. *72*, 343–379.

4. Bröer, S., and Palacín, M. (2011). The role of amino acid transporters in inherited and acquired diseases. Biochem. J. *436*, 193–211.

5. McCracken, A.N., and Edinger, A.L. (2013). Nutrient transporters: the Achilles' heel of anabolism. Trends Endocrinol. Metab. *24*, 200–208.

6. Fotiadis, D., Kanai, Y., and Palacín, M. (2013). The SLC3 and SLC7 families of amino acid transporters. Mol. Aspects Med. *34*, 139–158.

7. Kanai, R., Chaieb, L., Antal, A., Walsh, V., and Paulus, W. (2008). Frequency-dependent electrical stimulation of the visual cortex. Curr. Biol. *18*, 1839–1843.

8. Nicklin, P., Bergman, P., Zhang, B., Triantafellow, E., Wang, H., Nyfeler, B., Yang, H., Hild, M., Kung, C., Wilson, C., et al. (2009). Bidirectional transport of amino acids regulates mTOR and autophagy. Cell *136*, 521–534.

9. Verrey, F. (2003). System L: heteromeric exchangers of large, neutral amino acids involved in directional transport. Pflugers Arch. *445*, 529–533.

10. Cormerais, Y., Giuliano, S., LeFloch, R., Front, B., Durivault, J., Tambutté, E., Massard, P.A., de La Ballina, L.R., Endou, H., Wempe, M.F., et al. (2016). Genetic disruption of the multifunctional CD98/LAT1 complex demonstrates the key role of essential amino acid transport in the control of mTORC1 and tumor growth. Cancer Res. *76*, 4481–4492.

11. Elorza, A., Soro-Arnáiz, I., Meléndez-Rodríguez, F., Rodríguez-Vaello, V., Marsboom, G., de Cárcer, G., Acosta-Iborra, B., Albacete-Albacete, L., Ordóñez, A., Serrano-Oviedo, L., et al. (2012). HIF2α acts as an mTORC1 activator through the amino acid carrier SLC7A5. Mol. Cell *48*, 681–691.

12. Fuchs, B.C., and Bode, B.P. (2005). Amino acid transporters ASCT2 and LAT1 in cancer: partners in crime? Semin. Cancer Biol. *15*, 254–266.

13. Yue, M., Jiang, J., Gao, P., Liu, H., and Qing, G. (2017). Oncogenic MYC activates a feedforward regulatory loop promoting essential amino acid metabolism and tumorigenesis. Cell Rep. *21*, 3819–3832. https://doi.org/10.1016/j.celrep.2017.12.002.

14. de La Ballina, L.R., Cano-Crespo, S., González-Muñoz, E., Bial, S., Estrach, S., Cailleteau, L., Tissot, F., Daniel, H., Zorzano, A., Ginsberg, M.H., et al. (2016). Amino acid transport associated to cluster of differentiation 98 heavy chain (CD98HC) is at the cross-road of oxidative stress and amino acid availability. J. Biol. Chem. *291*, 9700–9711.

15. Kanai, Y., Segawa, H., Miyamoto, K.I., Uchino, H., Takeda, E., and Endou, H. (1998). Expression cloning and characterization of a transporter for large neutral amino acids activated by the heavy chain of 4F2 antigen (CD98). J. Biol. Chem. *273*, 23629–23632.

16. Cibrian, D., Saiz, M.L., de la Fuente, H., Sánchez-Díaz, R., Moreno-Gonzalo, O., Jorge, I., Ferrarini, A., Vázquez, J., Punzón, C., Fresno, M., et al. (2016). CD69 controls the uptake of L-tryptophan through LAT1-CD98 and AhR-dependent secretion of IL-22 in psoriasis. Nat. Immunol. *17*, 985–996.

17. Kundu, M., Lindsten, T., Yang, C.-Y., Wu, J., Zhao, F., Zhang, J., Selak, M.A., Ney, P.A., and Thompson, C.B. (2008). Ulk1 plays a critical role in the autophagic clearance of mitochondria and ribosomes during reticulocyte maturation. Blood *112*, 1493–1502.

18. Loftus, R.M., Assmann, N., Kedia-Mehta, N., O'Brien, K.L., Garcia, A., Gillespie, C., Hukelmann, J.L., Oefner, P.J., Lamond, A.I., Gardiner, C.M., et al. (2018). Amino acid-dependent cMyc expression is essential for NK cell metabolic and functional responses in mice. Nat. Commun. *9*, 2341.

19. Poncet, N., Mitchell, F.E., Ibrahim, A.F.M., McGuire, V.A., English, G., Arthur, J.S.C., Shi, Y.B., and Taylor, P.M. (2014). The catalytic subunit of the system L1 amino acid transporter (Slc7a5) facilitates nutrient signalling in mouse skeletal muscle. PLoS One *9*, e89547.

20. Sinclair, L. v, Rolf, J., Emslie, E., Shi, Y.B., Taylor, P.M., and Cantrell, D.A. (2013). Control of amino-acid transport by antigen receptors coordinates the metabolic reprogramming essential for T cell differentiation. Nat. Immunol. *14*, 500–508.

21. Kageyama, T., Nakamura, M., Matsuo, A., Yamasaki, Y., Takakura, Y., Hashida, M., Kanai, Y., Naito, M., Tsuruo, T., Minato, N., and Shimohama, S. (2000). The 4F2hc/LAT1 complex transports L-DOPA across the blood-brain barrier. Brain Res. *879*, 115–121.

22. Tărlungeanu, D.C., Deliu, E., Dotter, C.P., Kara, M., Janiesch, P.C., Scalise, M., Galluccio, M., Tesulov, M., Morelli, E., Sonmez, F.M., et al. (2016). Impaired amino acid transport at the blood brain barrier is a cause of autism spectrum disorder. Cell *167*, 1481–1494.e18.

23. Devés, R., and Boyd, C.A. (2000). Surface antigen CD98(4F2): not a single membrane protein, but a family of proteins with multiple functions. J. Membr. Biol. *173*, 165–177.

24. Fort, J., de La Ballina, L.R., Burghardt, H.E., Ferrer-Costa, C., Turnay, J., Ferrer-Orta, C., Usón, I., Zorzano, A., Fernández-Recio, J., Orozco, M., et al. (2007). The structure of human 4F2hc ectodomain provides a model for homodimerization and electrostatic interaction with plasma membrane. J. Biol. Chem. *282*, 31444–31452.

25. Bassi, M.T., Gasol, E., Manzoni, M., Pineda, M., Riboni, M., Martín, R., Zorzano, A., Borsani, G., and Palacín, M. (2001). Identification and characterisation of human xCT that co-expresses, with 4F2 heavy chain, the amino acid transport activity system xc-. Pflugers Arch. *442*, 286–296.

26. Bröer, A., Wagner, C.A., Lang, F., and Bröer, S. (2000). The heterodimeric amino acid transporter 4F2hc/y+LAT2 mediates arginine efflux in exchange with glutamine. Biochem. J. *349*, 787–795.

27. Fukasawa, Y., Segawa, H., Kim, J.Y., Chairoungdua, A., Kim, D.K., Matsuo, H., Cha, S.H., Endou, H., and Kanai, Y. (2000). Identification and characterization of a Na(+)-independent neutral amino acid transporter that associates with the 4F2 heavy chain and exhibits substrate selectivity for small neutral D- and L-amino acids. J. Biol. Chem. *275*, 9690–9698.

28. Pineda, M., Fernández, E., Torrents, D., Estévez, R., López, C., Camps, M., Lloberas, J., Zorzano, A., and Palacín, M. (1999). Identification of a membrane protein, LAT-2, that co-expresses with 4F2 heavy chain, an L-type amino acid transport activity with broad specificity for small and large zwitterionic amino acids. J. Biol. Chem. *274*, 19738–19744.

29. Sato, H., Tamba, M., Ishii, T., and Bannai, S. (1999). Cloning and expression of a plasma membrane cystine/glutamate exchange transporter composed of two distinct proteins. J. Biol. Chem. *274*, 11455–11458.

30. Torrents, D., Estévez, R., Pineda, M., Fernández, E., Lloberas, J., Shi, Y.B., Zorzano, A., and Palacín, M. (1998). Identification and characterization of a membrane protein (y+L amino acid transporter-1) that associates with 4F2hc to encode the amino acid transport activity y+L. A candidate gene for lysinuric protein intolerance. J. Biol. Chem. *273*, 32437–32445.

31. Doulatov, S., Notta, F., Laurenti, E., and Dick, J.E. (2012). Hematopoiesis: a human perspective. Cell Stem Cell *10*, 120–136.

32. Dzierzak, E., and Philipsen, S. (2013). Erythropoiesis: development and differentiation. Cold Spring Harb. Perspect. Med. *3*, a011601.

33. Eaves, C.J. (2015). Hematopoietic stem cells: concepts, definitions, and the new reality. Blood *125*, 2605–2613.

34. Higgins, J.M. (2015). Red blood cell population dynamics. Clin. Lab. Med. *35*, 43–57.

35. Gregory, C.J., and Eaves, A.C. (1977). Human marrow cells capable of erythropoietic differentiation in vitro: definition of 3 erythroid colony responses. Blood *49*, 855–864.

36. Stephenson, J.R., Axelrad, A.A., McLeod, D.L., and Shreeve, M.M. (1971). Induction of colonies of hemoglobin-synthesizing cells by erythropoietin in vitro. Proc. Natl. Acad. Sci. USA *68*, 1542–1546.

37. Chen, K., Liu, J., Heck, S., Chasis, J.A., An, X., and Mohandas, N. (2009). Resolving the distinct stages in erythroid differentiation based on dynamic changes in membrane protein expression during erythropoiesis. Proc. Natl. Acad. Sci. USA *106*, 17413–17418.

38. Liu, J., Zhang, J., Ginzburg, Y., Li, H., Xue, F., de Franceschi, L., Chasis, J.A., Mohandas, N., and An, X. (2013). Quantitative analysis of murine terminal erythroid differentiation in vivo:novelmethod to study normal and disordered erythropoiesis. Blood *121*, e43–e49.

39. Chen, J.J., and Zhang, S. (2019). Heme-regulated eIF2α kinase in erythropoiesis and hemoglobinopathies. Blood *134*, 1697–1707.

40. Honda, S., Arakawa, S., Nishida, Y., Yamaguchi, H., Ishii, E., and Shimizu, S. (2014). Ulk1-mediated Atg5-independent macroautophagy mediates elimination of mitochondria from embryonic reticulocytes. Nat. Commun. *5*, 4004–4013.

41. Kent, G., Minick, O.T., Volini, F.I., and Orfei, E. (1966). Autophagic vacuoles in human red cells. Am. J. Pathol. *48*, 831–857.

42. Moras, M., Lefevre, S.D., and Ostuni, M.A. (2017). From erythroblasts to mature red blood cells: organelle clearance in mammals. Front. Physiol. *8*, 1076.

43. Pishesha, N., Thiru, P., Shi, J., Eng, J.C., Sankaran, V.G., and Lodish, H.F. (2014). Transcriptional divergence and conservation of human and mouse erythropoiesis. Proc. Natl. Acad. Sci. USA *111*, 4103–4108.

44. An, X., Schulz, V.P., Mohandas, N., and Gallagher, P.G. (2015). Human and murine erythropoiesis. Curr. Opin. Hematol. 22, 206–211.

45. Nandakumar, S.K., Ulirsch, J.C., and Sankaran, V.G. (2016). Advances in understanding erythropoiesis: evolving perspectives. Br. J. Haematol. 173, 206–218.

46. Paulson, R.F., Shi, L., and Wu, D.C. (2011). Stress erythropoiesis: new signals and new stress progenitor cells. Curr. Opin. Hematol. 18, 139–145.

47. Socolovsky, M. (2007). Molecular insights into stress erythropoiesis. Curr. Opin. Hematol. 14, 215–224.

48. Franke, K., Kalucka, J., Mamlouk, S., Singh, R.P., Muschter, A., Weidemann, A., Iyengar, V., Jahn, S., Wieczorek, K., Geiger, K., et al. (2013). HIF-1α is a protective factor in conditional PHD2-deficient mice suffering from severe HIF-2α-induced excessive erythropoiesis. Blood 121, 1436–1445.

49. Gassmann, M., and Muckenthaler, M.U. (2015). Adaptation of iron requirement to hypoxic conditions at high altitude. J. Appl. Physiol. 119, 1432–1440.

50. Gruber, M., Hu, C.J., Johnson, R.S., Brown, E.J., Keith, B., and Simon, M.C. (2007). Acute postnatal ablation of Hif-2α results in anemia. Proc. Natl. Acad. Sci. USA 104, 2301–2306.

51. Koury, M.J., and Haase, V.H. (2015). Anaemia in kidney disease: harnessing hypoxia responses for therapy. Nat. Rev. Nephrol. 11, 394–410.

52. Lorenzo, F.R., Huff, C., Myllymäki, M., Olenchock, B., Swierczek, S., Tashi, T., Gordeuk, V., Wuren, T., Ri-Li, G., McClain, D.A., et al. (2014). A genetic mechanism for Tibetan high-altitude adaptation. Nat. Genet. 46, 951–956.

53. Haase, V.H. (2013). Regulation of erythropoiesis by hypoxia-inducible factors. Blood Rev. 27, 41–53.

54. Kobayashi, H., Liu, Q., Binns, T.C., Urrutia, A.A., Davidoff, O., Kapitsinou, P.P., Pfaff, A.S., Olauson, H., Wernerson, A., Fogo, A.B., et al. (2016). Distinct subpopulations of FOXD1 stroma-derived cells regulate renal erythropoietin. J. Clin. Invest. 126, 1926–1938.

55. Shih, H.M., Wu, C.J., and Lin, S.L. (2018). Physiology and pathophysiology of renal erythropoietin-producing cells. J. Formos. Med. Assoc. 117, 955–963.

56. Bunn, H.F. (2013). Erythropoietin. Cold Spring Harb. Perspect. Med. 3, a011619.

57. Elliott, S., and Sinclair, A.M. (2012). The effect of erythropoietin on normal and neoplastic cells. Biologics 6, 163–189.

58. Iscove, N.N., Sieber, F., and Winterhalter, K.H. (1974). Erythroid colony formation in cultures of mouse and human bone marrow: analysis of the requirement for erythropoietin by gel filtration and affinity chromatography on agarose-concanavalin A. J. Cell. Physiol. 83, 309–320.

59. Sawada, K., Krantz, S.B., Dai, C.H., Koury, S.T., Horn, S.T., Glick, A.D., and Civin, C.I. (1990). Purification of human blood burst-forming units-erythroid and demonstration of the evolution of erythropoietin receptors. J. Cell. Physiol. 142, 219–230.

60. Wojchowski, D.M., Gregory, R.C., Miller, C.P., Pandit, A.K., and Pircher, T.J. (1999). Signal transduction in the erythropoietin receptor system. Exp. Cell Res. 253, 143–156.

61. Koulnis, M., Pop, R., Porpiglia, E., Shearstone, J.R., Hidalgo, D., and Socolovsky, M. (2011). Identification and analysis of mouse erythroid progenitors using the CD71/TER119 flow-cytometric assay. J. Vis. Exp. e2809.

62. Cibrian, D., Castillo-González, R., Fernández-Gallego, N., de la Fuente, H., Jorge, I., Saiz, M.L., Punzón, C., Ramírez-Huesca, M., Vicente-Manzanares, M., Fresno, M., et al. (2020). Targeting L-type amino acid transporter 1 in innate and adaptive T cells efficiently controls skin inflammation. J. Allergy Clin. Immunol. 145, 199–214.e11.

63. Ohgaki, R., Ohmori, T., Hara, S., Nakagomi, S., Kanai-Azuma, M., Kaneda-Nakashima, K., Okuda, S., Nagamori, S., and Kanai, Y. (2017). Essential roles of L-type amino acid transporter 1 in syncytiotrophoblast development by presenting Fusogenic 4F2hc. Mol. Cell Biol. 37. e004277-16-e516.

64. Heinrich, A.C., Pelanda, R., and Klingmüller, U. (2004). A mouse model for visualization and conditional mutations in the erythroid lineage. Blood 104, 659–666.

65. Tauzin, L., Campos, V., and Tichet, M. (2018). Cellular endogenous NAD(P)H fluorescence as a label-free method for the identification of erythrocytes and reticulocytes. Cytometry A. 93, 472–479.

66. Knight, Z.A., Schmidt, S.F., Birsoy, K., Tan, K., and Friedman, J.M. (2014). A critical role for mTORC1 in erythropoiesis and anemia. Elife 3, e01913.

67. Sonenberg, N., and Hinnebusch, A.G. (2009). Regulation of translation initiation in eukaryotes: mechanisms and biological targets. Cell 136, 731–745.

68. Creed, S., and McKenzie, M. (2019). Measurement of mitochondrial membrane potential with the fluorescent dye tetramethylrhodamine methyl ester (TMRM). Methods Mol. Biol. 1928, 69–76.

69. Milkereit, R., Persaud, A., Vanoaica, L., Guetg, A., Verrey, F., and Rotin, D. (2015). LAPTM4b recruits the LAT1-4F2hc Leu transporter to lysosomes and promotes mTORC1 activation. Nat. Commun. 6, 7250.

70. Arlet, J.B., Dussiot, M., Moura, I.C., Hermine, O., and Courtois, G. (2016). Novel players in β-thalassemia dyserythropoiesis and new therapeutic strategies. Curr. Opin. Hematol. 23, 181–188.

71. Palis, J. (2014). Primitive and definitive erythropoiesis in mammals. Front. Physiol. 5, 3.

72. Riley, R.S., Ben-Ezra, J.M., Goel, R., and Tidwell, A. (2001). Reticulocytes and reticulocyte enumeration. J. Clin. Lab. Anal. 15, 267–294.

73. Betsunoh, H., Fukuda, T., Anzai, N., Nishihara, D., Mizuno, T., Yuki, H., Masuda, A., Yamaguchi, Y., Abe, H., Yashi, M., et al. (2013). Increased expression of system large amino acid transporter (LAT)-1 mRNA is associated with invasive potential and unfavorable prognosis of human clear cell renal cell carcinoma. BMC Cancer 13, 509.

74. Higuchi, K., Sakamoto, S., Ando, K., Maimaiti, M., Takeshita, N., Okunushi, K., Reien, Y., Imamura, Y., Sazuka, T., Nakamura, K., et al. (2019). Characterization of the expression of LAT1 as a prognostic indicator and a therapeutic target in renal cell carcinoma. Sci. Rep. 9, 16776.

75. Perkins, C.P., Mar, V., Shutter, J.R., del Castillo, J., Danilenko, D.M., Medlock, E.S., Ponting, I.L., Graham, M., Stark, K.L., Zuo, Y., et al. (1997). Anemia and perinatal death result from loss of the murine ecotropic retrovirus receptor mCAT-1. Genes Dev. 11, 914–925.

76. Zhang, Q., Steensma, D.P., Yang, J., Dong, T., and Wu, M.X. (2019). Uncoupling of CD71 shedding with mitochondrial clearance in reticulocytes in a subset of myelodysplastic syndromes. Leukemia 33, 217–229.

77. Rodríguez-García, R., López-Montero, I., Mell, M., Egea, G., Gov, N.S., and Monroy, F. (2015). Direct cytoskeleton forces cause membrane softening in red blood cells. Biophys. J. 108, 2794–2806.

78. Wolfram Research, Inc., Mathematica, Version 13.1, Champaign, IL (2022)

79. Wolfram Research (2010). Component measurements, Wolfram Language function. updated 2017. https://reference.wolfram.com/language/ref/ComponentMeasurements.html.

STAR★METHODS

KEY RESOURCES TABLE

REAGENT or RESOURCE	SOURCE	IDENTIFIER
Antibodies		
Rat monoclonal Biotin Anti-Mouse CD71	BioLegend	Cat# 113803, RRID:AB_313564
Rat monoclonal Anti-Mouse CD16/CD32	Tonbo Biosciences	Cat#70-0161, RRID:AB_2621487
Rat monoclonal PE Anti-Mouse CD71	BD Pharmingen	Cat#553267, RRID:AB_394744
Rat monoclonal Biotin Anti-Mouse TER-119	Tonbo Biosciences	Cat#30-5921, RRID:AB_2621651
Rat monoclonal APC Anti-Mouse CD98 (4F2)	BioLegend	Cat#128211, RRID:AB_2750544
Rat monoclonal κ Isotype APC Ctrl Antibody	BioLegend	Cat#400526, RRID:AB_2864284
Rat monoclonal PE/Cy7 Anti-Mouse CD98 (4F2)	BioLegend	Cat# 128213, RRID:AB_2750546
Rat monoclonal PE/Cy7 Anti-Mouse CD98 (4F2)	BioLegend	Cat#128211, RRID:AB_2750544
Rat monoclonal APC Anti-Mouse CD71	BD Biosciences	Cat#567258
Rabbit monoclonal Pacific Blue Anti-Mouse Phospho-S6 Ribosomal Protein (Ser235/236)	Cell Signaling Technology	Cat#8520, RRID:AB_2797646
Mouse monoclonal PerCP Anti-Human CD45	BD Biosciences	Cat#345809, RRID:AB_2868830
Mouse monoclonal APC-H7 Anti-Human CD71	BD Biosciences	Cat#655431, RRID:AB_2870381
Mouse monoclonal PE Anti-Human Glycophorin A	BD Biosciences	Cat#340947, RRID:AB_400188
Rabbit polyclonal Anti-LAT1 (SLC7A5)	Alomone Labs	Cat# ANT-105, RRID:AB_2756724
Mouse Monoclonal Anti-beta-Actin-Peroxidase	Sigma Aldrich	Cat# A3854, RRID:AB_262011
Biological samples		
Whole fresh blood from healthy or anemic human donors	They were obtained and analyzed in Immunology Department of Hospital de la Princesa, Madrid, (Spain).	N/A
Whole fresh blood of mice	They were obtained from erythroid Slc7a5-deficient and control mice housed in the Animal Facility of Autonomous University of Madrid (UAM).	N/A
Spleen of mice	They were obtained from erythroid Slc7a5-deficient and control mice housed in the Animal Facility of Autonomous University of Madrid (UAM).	N/A
Chemicals, peptides, and recombinant proteins		
γ-Globulins from human blood	Sigma Aldrich	Cat#G4386
Phenylhydrazine hydrochloride	Merck	Cat#114715
Binocrit® recombinant human EPO (rh-EPO)	Sandoz GmbH	Eprex/Erypo
Temsirolimus	Sigma-Aldrich	Cat#PZ0020
Hoechst 33342	Sigma-Aldrich	Cat#B2261
Alexa Fluor 488-conjugated streptavidin	Molecular Probes	Cat#S32354
Pacific Blue-conjugated streptavidin	Invitrogen	Cat#S11222
DRAQ5	Thermo Fisher Scientific	Cat#62251
Tetramethylrhodamine methyl ester (TMRM)	Thermo Fisher Scientific	Cat#T668
MitoTracker Green	Thermo Fisher Scientific	Cat#T668

Continued

REAGENT or RESOURCE	SOURCE	IDENTIFIER
Critical commercial assays		
Mouse Erythropoietin ELISA Quantikine Immunoassay kit	R&D Systems	Cat#MEP00B
Experimental models: Organisms/strains		
Mouse: *Cre* knock-in line (*ErGFPcre*)	Provided by Dr Ursula Klingmüller (Heinrich et al., 2014[64])	N/A
Mouse: *Slc7a5*^{LoxP/LoxP} with *LoxP* sites flank exon 1 of the murine Slc7a5 locus	Provided by Dr Peter Taylor (Poncet et al., 2014[19])	N/A
ErGFPcre Slc7a5^{LoxP/LoxP} mice	This manuscript	N/A
Oligonucleotides		
Primer: *Epo* Forward: CAAAGTAACTTCTATGCTTGGAAAA.	Condalab	N/A
Primer: *Epo* Reverse, 5′-CAGGCCTTGCCAAACTTCTATG-3′	Condalab	N/A
Primer: *Slc7a5* Forward: TTCGCCACCTACTTGCTCAA.	Condalab	N/A
Primer: *Slc7a5* Reverse 5′-CCTTTACGCTGTAGCAGTTC-3′	Condalab	N/A
Primer: *28S* Forward: GGTAGCCAAATGCCTCGTCAT. reverse 5′-GGATAGTAGGTAGGGACAGTGGGAAT-3′	Condalab	N/A
Primer: *28S* Reverse 5′-GGATAGTAGGTAGGGACAGTGGGAAT-3′	Condalab	N/A
Primer for amplification of murine genomic region lacking *Slc7a5* exon1 in *ErGFPcre Slc7a5*^{LoxP/LoxP} mice Forward: 5′-GGCTCCTGGACTTATCTTGACCAATG-3′.	Poncet el at. 2014[19]	N/A
Primer for amplification of murine genomic region lacking *Slc7a5* exon1 in *ErGFPcre Slc7a5*^{LoxP/LoxP} mice Reverse, 5′-GTGGTGCTTTGCTGAAGGCAGGG-3′	Poncet el at. 2014[19]	N/A
Software and algorithms		
QuantStudio5 Design and Analysis Software v1.4	Applied Biosystems	RRID:SCR_020240
ImageJ	NIH	RRID:SCR_003070
BD FACSDiva™ software	BD Biosciences	RRID:SCR_001456
FlowJo™ v10.7 software	BD Biosciences	RRID:SCR_008520
GraphPad Prism software	GraphPad	RRID:SCR_002798
Wolfram Mathematica	Wolfram Mathematica	RRID:SCR_014448

RESOURCE AVAILABILITY

Lead contact
Further information and requests for resources and reagents should be directed to and will be fulfilled by the lead contact, Julián Aragonés López (julian.aragones@uam.es).

Materials availability
ErGFPcre mice were provided by Dr Ursula Klingmüller under conditions of a Material Transfer agreement. *Slc7a5*^{LoxP/LoxP} mice provided by Dr. Peter Taylor are now available in The Jackson Laboratory (Slc7a5^{fl} #027252).

Data and code availability

- Data reported in this paper will be shared by the lead contact upon request.

- This paper does not report original code.

- Any additional information required to reanalyze the data reported in this paper is available from the lead contact upon request.

EXPERIMENTAL MODEL AND SUBJECT DETAILS

Mouse models

All experimental procedures involving mice were first approved by the research ethics committee at the Autonomous University of Madrid (UAM - CEIC 55-1002-A049, approval date ninth May 2014 and CEIC 103-1993-341 approval date 25th November 2019). All the procedures were carried out in male and female mice under the supervision of the animal welfare personnel at the UAM, and in accordance with Spanish RD 53/2013 and European (EU Directive 2010/63/EU) guidelines. Mice were used with an age between 8 and 48 weeks. Each experiment was performed with mice of similar age. *ErGFPcre* mice that express the Cre recombinase under the control of the EPOR promoter were provided by Dr Ursula Klingmüller (Deutsches Krebsforschungszentrum -DKFZ, German Cancer Research Center, Heidelberg Germany: Heinrich et al., 2014).[64] These mice were crossed with *Slc7a5$^{LoxP/LoxP}$* mice, in which *LoxP* sites flank exon 1 of the murine *Slc7a5* locus, to generate *ErGFPcre Slc7a5$^{LoxP/LoxP}$* mice. The *Slc7a5$^{LoxP/LoxP}$* mice were provided by Dr Peter Taylor (University of Dundee, Dundee, United Kingdom).[19]

Patient samples

The analysis on human samples from males and females was performed in accordance with the principles of the Declaration of Helsinki and was approved and supervised by the Ethics Committee of Instituto de Investigación del Hospital Universitario de la Princesa. For this analysis we used whole fresh blood from subjects with iron-deficient or post-chemotherapy anemia or healthy donors with an age between 22 and 86 years. Blood (2 μL) was blocked with 100 mg/mL of human γ-globulin (Sigma-Aldrich, St. Louis, MO, USA) for 30 min. The samples were then stained with 100 μL of a mouse anti-human SLC3A2 (CD98) mAb (clone 4F2) for 30 min and after washing, they were incubated for 30 min with an Alexa Fluor 488 conjugated goat anti-mouse secondary antiserum (1:100, Invitrogen, Waltham, MA, USA). After another washing step, the samples were further stained for 30 min with the following mouse anti-human mAbs: CD45-PerCP (clone 2D1), CD71-APC-H7 (clone M-A712), Glycophorin A-PE (clone GA-R2 -HIR2) (all from BD Biosciences, Franklin Lakes, NJ, USA). The CD45-PerCP (clone 2D1) was used to exclude leukocytes in the analysis. Samples were then acquired on a BD FACSCanto II and analyzed with the FlowJoTM v10.7 software.

METHOD DETAILS

RT-PCR, PCR analysis and primers

The total RNA from cells was isolated with Ultraspec or TRIsure (BIO-38032, Bioline USA, Inc., Memphis, TN, USA) and this RNA (1 μg) was then reverse-transcribed using Improm-II reverse transcriptase (Promega, Madison, WI, USA). Polymerase chain reaction (PCR) amplifications were performed using the Power SYBR Green PCR Master Mix kit (Applied Biosystems, Foster City, CA, USA) in a QuantStudio5 (Applied Biosystems, Foster City, CA, USA) with the primer sets indicated below. The data were analyzed with QuantStudio5 Design and Analysis Software v1.4 (Applied Biosystems, Foster City, CA, USA). The following set of primers were used: *Epo* (forward 5′ -CAAA GTAACTTCTATGCTTGGAAAA-3′ reverse, 5′-CAGGCCTTGCCAAACTTCTATG-3′); *Slc7a5* (forward 5′-TTC GCCACCTACTTGCTCAA-3′, reverse 5′-CCTTTACGCTGTAGCAGTTC-3′); *28S* (forward 5′-GGTAGCCAAATG CCTCGTCAT-3′, reverse 5′-GGATAGTAGGTAGGGACAGTGGGAAT-3′). For amplification of murine genomic region lacking *Slc7a5* exon1 in *ErGFPcre Slc7a5$^{LoxP/LoxP}$* mice the following primers were used forward 5′-GGCTCCTGGACTTATCTTGACCAATG-3′ reverse, 5′- GTGGTGCTTTGCTGAAGGCAGGG-3′).[19]

Phenylhydrazine (PHZ) treatment, phlebotomy, rhEPO administration and temsirolimus treatment

Phenylhydrazine hydrochloride (PHZ: Merck KGaA, Darmstadt, Germany) was prepared in PBS (pH 7.2) at 18 mg/mL and it was administered intraperitoneally (ip) in a single 40 μg/g dose. Phlebotomy was performed by three consecutive submandibular punctures, each at an interval of 24h. Mice were treated

with two doses PHZ 60 μg/g in two days or a dose of PHZ 80 μg/g for western blot and oxygen consumption analysis respectively. These higher doses of PHZ results in blood samples in which a larger proportion of red blood cells are reticulocytes. For the treatment with recombinant human EPO (rhEPO, Epoetina, Binocrit), 200 U of rhEPO was administered by two consecutive days. Flow cytometry and RT-PCR analysis were performed two days after the first injection. Temsirolimus (Sigma-Aldrich, St Louis, MO, USA) was solubilized at a 4 mg/mL stock solution in DMSO. The following two days after PHZ treatment, mice were treated by intraperitoneal (ip) injection with temsirolimus (20 mg/kg) each day or with the same volume of DMSO as control. Flow cytometry analysis was performed the following day after temsirolimus treatment.

Hematological analysis

Blood was collected into EDTA K3-coated microcapillaries (Sarstedt Inc., Nümbrecht, Germany), and the hematocrit (%), hemoglobin (g/dL), RBC count (x10^6 cells/μl), mean corpuscular volume (MCV, μm^3) and mean corpuscular hemoglobin (MCH, pg) was determined in an ABX Pentra 80 analyzer (Horiba Medical, Madrid, Spain). A parallel RBC count was also performed using a cell counter (EVETM PLUS Automated cell counter, Nanoentek, Guro-gu, South Korea). May-Grünwald-Giemsa staining was performed as follows: initial staining with May-Grünwald reagent (eosin, methylene blue, methanol, glycerol) for 5 min; after the pigment was removed, Giemza staining (azure II, eosin, methanol, glycerol) was performed for 25 min. After washing and drying, cells were evaluated using a light microscopy with attached camera (Leica DMC2900, Leica Biosystems; Germany).

Life imaging morphology cytometry (LIMC)

Fresh blood samples were aliquoted (20 μL) and mixed with PBS+ buffer (500 μL). The suspension PBS was composed of NaCl (130 mM) and Na$_3$PO$_4$ (20 mM) supplemented with glucose (10 mM); hereinafter named PBS+ buffer. These components were first dissolved in distilled water, then, pH was adjusted to 7.4, and BSA was finally added under mild stirring (BSA 1 mg/mL). NaCl (Sigma-Aldrich, MO, USA), Na$_3$PO$_4$ (Sigma-Aldrich, MO, USA), Glucose (Riedel-de Haën, USA), BSA (Sigma-Aldrich, MO, USA). This enriched physiological buffer does not contain exogenously added ATP but supports endogenous ATP-production through glycolysis.[77] The RBC suspensions were 3-fold centrifuged (5000 rpm for 10 min at room temperature) and further rinsed in PBS+ buffer. The erythrocytes were concentrated and leukocyte and platelet supernatants were separated from the pelleted fraction. The RBC pellet (20 μL) was resuspended prior use in PBS+ buffer (480 μL). To prepare living RBC smears a drop of the diluted RBC suspension (10 μL) was poured on a microscopy slide placed on the observation chamber (at 37°C), which was immediately sealed with a cover glass to avoid evaporation and uncontrolled osmotic stress. No chromogenic staining nor fluorescent staining were considered in order to preserve the RBCs in a living status. These living RBC smears were processed for imaging immediately after preparation.

For life imaging morphology cytometry (LIMC), the living RBC smears were photographed using an inverted Nikon 80i microscope (Tokyo, Japan) in the phase contrast mode (PlanApo oil immersion objective 100x, N.A. 1.45, zoom telescope 1.5x). The LIMC platform was equipped with an ultrafast sCMOS camera (FastCAM SA3, Photron, Tokyo, Japan; 200 kfps maximal rate, 1 Mpixel; 12 Gbytes RAM). LIMC is a cytometric *in vitro* tool allowing to assess morphological living cell phenotypes to gain quantitative appreciation on cell size and shape heterogeneities as appeared in physiological milieu. Per each RBC phenotype we scanned more than ten different smear emplacements in at least three slides. For image post-processing: 3D-cell rendering, we detected each RBC specimen by using a binary image segmentation approach, followed by a detailed morphological analysis of the segmented components. All the scripts were constructed in Wolfram Language.[78] A soft noise reduction step was first performed by processing the raw images through of a Gaussian kernel (two pixels radius). This pre-filtering is followed by an intensity rescaling to cover the range from 0 to 1. The segmentation process started with the detection of the phase contrast halo surrounding each cell, defined as the positions of the pixels whose intensities locate in the upper quartile of the intensity histogram. Then, a binary segmentation of the color negated image was performed by using the Kapur's histogram entropy minimization method (Kapur et al., 1985). In order to reliable morphological analysis, a filling transform of the binarized components were performed, discarding small components as well as any element in the border of the image.[79] Finally, the binary mask was applied to the original image.

For each single RBC both morphological (projected area, perimeter, elongation and circularity) and optical (mean intensity, entropy and SD) properties were extracted. Some representative specimens were selected

for image post-processing in which a pseudo-3D reconstruction is performed allowing better visualization of the real cell volume as rendered from 2D images. The algorithm is based on a relief image where x-y image intensities represent z elevations. For better description of the central concavity of the discocytes, we exploit 3D-rendering that combines the raw image for the external area and its negative for the central region. Morphological and size parameters were expressed as populational means and their standard deviations determined for size different animals per phenotype.

Amino acid uptake assay

Circulating CD71^{HI}/Ter119^{HI} reticulocytes were isolated from whole blood of PHZ-treated control and ErGFPcre *Slc7a5$^{LoxP/LoxP}$* mice by using the EasySep Release Mouse Biotin Positive Selection Kit and the EasySep Magnet (17,655, 18,000, StemCell Technologies, Vancouver, Canada) according to the manufacturer's instructions. Briefly, approximately 1x10^8 cells were incubated with a Biotin anti-mouse CD71 Antibody (2 µg/µL dilution: 113,803, BioLegend, San Diego, CA, USA) and streptavidin-coated magnetic particles. Circulating CD71^{HI}/Ter119^{HI} reticulocytes cells were positively selected and resuspended in RPMI 1640 Medium (Gibco, Carlsbad, CA, USA). For amino acid uptake assay cells were switched to RPMI 1640 Medium diluted 1/10 into RPMI 1640 Medium w/o Amino Acids (US Biological, Swampscott, MA, USA) in order to dilute cold L-phenylalanine to a final concentration of 9.1 µmol/L. The ^{3}H-radiolabeled amino acid L-phenylalanine (PerkinElmer, Waltham, MA, USA) was added (0.5 µCi/mL) at a final extracellular concentration of 5 µmol/L. Amino acid uptake was measured after an o/n incubation at 37°C. Uptake was stopped by addition of 20 mmol/L cold L-Leu to quench L-System. Then, cells were harvested onto glass-fiber filter using a Tomtec 96-well parallel harvester (Tomtec, Hamden, CT, USA). B-radioactivity was counted in a Beckman LS 6500 Multi-Purpose Scintillation Counter (Beckman Coulter, Fullerton, CA, USA).

Oxygen consumption measurements

Oxygen consumption rate was measured through a glucose-based mitostress test in an XF-96 Extracellular Flux Analyzer (Seahorse Bioscience) in 6.5x10^6 red blood cells from PHZ-treated control and *ErGFPcre Slc7a5$^{LoxP/LoxP}$* mice. Three consecutive mix and measure steps were performed for resting conditions and after each injection (3 min each). Cells were cultured in DMEM medium (D5030, Sigma Aldrich) supplemented with 2 mM sodium pyruvate, 2 mM L-glutamine and 25 mM glucose) followed by the addition of oligomycin (2.5 µM), fluoro-carbonyl cyanide phenylhydrazone (FCCP; 3 µM) in order to measure maximal oxygen consumption, and finally rotenone/antimycin A (4 µM each).

Flow cytometry

Spleen fragments were filtered through sterile 70 µm pore cell strainers (431,751, Corning Inc., Nueva York, NY, USA). Splenic and/or peripheral blood cells were suspended in PBS (PBS) supplemented with 1% fetal bovine serum (FBS) and 1% EDTA 0.5M. For the flow cytometry analysis, cells were stained with anti-mouse CD16/CD32 (1:100 dilution: 70–0161, Tonbo Biosciences, San Diego, CA, USA) and Hoechst 342 (:10,000 dilution: H33342 B2261, Sigma-Aldrich, St. Louis, MO, USA). For SLC3A2 flow cytometry analysis in the different erythroid cell populations the following antibodies (diluted 1:100) were used: (PE)-conjugated anti-mouse CD71 (553,267, BD Pharmingen, Franklin Lakes, NJ, USA); Biotin anti-mouse TER-119 (30-5921-U500, Tonbo Biosciences, San Diego, CA, USA); APC-conjugated SLC3A2 (CD98) (4F2: 128,211, 128,213, BioLegend, San Diego, CA, USA); APC-conjugated IgG (400,526, BioLegend, San Diego, CA, USA). To detect the Biotin anti-mouse TER-119 antibody, Alexa Fluor 488-conjugated streptavidin (S32354, Invitrogen, Waltham, MA, USA) was used at a 1:200 dilution. For combined SLC3A2 and DRAQ5 flow cytometry analysis, cells were stained with (PE)-conjugated anti-mouse CD71 (1:100 dilution), Biotin anti-mouse TER-119 (1:100 dilution), PE/Cy7-conjugated SLC3A2 (CD98) (1:100 dilution: 4F2: 128,211, 128,213, BioLegend, San Diego, CA, USA), IgG Pe-Cy7 IgG (1:100 dilution: 400,526, BioLegend, San Diego, CA, USA) and DRAQ5 (1:5,000 dilution: 62,251, Thermo Fisher, Waltham, MA, USA). To detect the Biotin anti-mouse TER-119 antibody, Alexa Fluor 488-conjugated streptavidin (1:200 dilution) was used. For TMRM analysis, (APC)-conjugated anti-mouse CD71 (1:100 dilution: 567,258, BD Pharmingen, Franklin Lakes, NJ, USA); Biotin anti-mouse TER-119 and tetramethylrhodamine methyl ester probe (TMRM, 200 nM: T668, Thermo Fisher, Waltham, MA, USA) were used. The Biotin anti-mouse TER-119 antibody was detected using Alexa Fluor 488-conjugated streptavidin (1:200 dilution). For MitoTracker Green analysis, (PE)-conjugated anti-mouse CD71 (553,267, BD Pharmingen, Franklin Lakes, NJ, USA); Biotin anti-mouse TER-119 and MitoTracker Green FM (MitoTracker Green, 20 nM: T668, Thermo Fisher, Waltham, MA, USA) were used. To detect the Biotin anti-mouse TER-119 antibody, Pacific Blue-conjugated streptavidin (S11222, Invitrogen, Waltham, MA, USA) was used at a 1:200 dilution. For

Phospho-S6 Ribosomal Protein analysis, cells were first fixed with Paraformaldehyde (PFA) 1% and Glutaraldehyde 0.0075% for 10 min. Then, cells were permeabilized with 0.005% saponin for 10 min. After the fixation and permeabilization protocol, cells were stained with (PE)-conjugated anti-mouse CD71 (1:100 dilution), Biotin anti-mouse TER-119 (1:100 dilution), Pacific Blue-conjugated Phospho-S6 Ribosomal Protein (Ser235/236) (1:100 dilution: 8520S, Cell Signaling Technology, Danvers, MA, USA) and DRAQ5 (1:5,000 dilution). The Biotin anti-mouse TER-119 antibody was detected using Alexa Fluor 488-conjugated streptavidin (1:200 dilution). Cell fluorescence was analyzed on a FACSCanto™ II flow cytometer (BD Biosciences, Franklin Lakes, NJ, USA), and the data were analyzed with the BD FACSDiva™ software and BD FlowJo™ v10.7 software. Histograms are normalized to mode.

Serum EPO measurement

EPO was measured in serum samples under basal conditions, as well as in PHZ-treated mice, with a Mouse Erythropoietin ELISA Quantikine Immunoassay kit (MEP00B, R&D Systems, Minneapolis, MN, USA). Serum samples from basal conditions were diluted 1/3 with RD6Z calibrator diluent and those from PHZ-treated mice 1/15. Each dilution was incubated overnight with the RD1W assay diluent in polystyrene microplates precoated with a monoclonal antibody specific for mouse EPO and thereafter the manufacturers' protocol was followed. Optic density was measured on a Spectra MR spectrophotometer (29,010, Dynex Technologies, Chantilly, VA, USA).

Western blot analysis

Cells were lysed in Laemmli buffer, and the non-heated protein extract was resolved on 10% SDS-polyacrylamide gels and transferred to 0.45 μm nitrocellulose membranes. The membranes were then blocked and probed with antibodies against: LAT1 (SLC7A5) (ANT-105, Alomone Labs, Jerusalem, Israel); β-actin (A3854, Sigma-Aldrich). Antibody binding was detected by enhanced chemiluminiscence (Clarity, BioRad; and Super-Signal West Femto Maximum Sensitivity Substrate, Thermo Fisher, Waltham, MA, USA) and visualized on a digital luminescent image analyzer (Image Quant LAS4000 Mini; GE Healthcare, Chicago, IL, USA).

QUANTIFICATION AND STATISTICAL ANALYSIS

The data were expressed as the mean ± SEM (SEM). Statistical analysis was performed using one-way ANOVA followed by Tukey's post hoc test when comparing three groups or two-tailed Student's *t* test with Welch's correction when comparing two groups. All statistical analyses were performed using GraphPad Prism software (San Diego, CA, USA).